



1 Assimilation of citizen science data in snowpack modeling using a new 2 snow dataset: Community Snow Observations

3
4 **Ryan L. Crumley¹, David F. Hill², Katreen Wikstrom Jones³, Gabriel J. Wolken^{3,4}, Anthony A.
5 Arendt⁵, Christina M. Aragon¹, Christopher Cosgrove⁶, Community Snow Observations Participants⁷**

6
7 ¹Water Resources Science, Oregon State University, Corvallis, OR 97331, USA
8 ²School of Civil and Construction Engineering, Oregon State University, Corvallis, OR 97331, USA
9 ³Alaska Division of Geological and Geophysical Surveys, Fairbanks, AK 99709, USA
10 ⁴International Arctic Research Center, University of Alaska Fairbanks, Fairbanks, AK 99775, USA
11 ⁵University of Washington, Applied Physics Laboratory, WA 98105, USA
12 ⁶Geography Department, Oregon State University, Corvallis, OR 97331, USA
13 ⁷Citizen scientists participating in the project Community Snow Observations (CSO)

14
15
16
17 *Correspondence to:* Ryan L. Crumley (ryanlcrumley@gmail.com)

18 **Abstract.**

19
20
21 A physically-based snowpack evolution and redistribution model was used to test the effectiveness of assimilating crowd-sourced
22 measurements of snow depth by citizen scientists. The Community Snow Observations (CSO; communitysnowobs.org) project
23 gathers, stores, and distributes measurements of snow depth recorded by recreational users and snow professionals in high
24 mountain environments. These citizen science measurements are valuable since they come from terrain that is relatively under-
25 sampled and can offer *in-situ* snow information in locations where snow information is sparse or non-existent. The present study
26 investigates 1) the improvements to model performance when citizen science measurements are assimilated and 2) the number of
27 measurements necessary to obtain those improvements. Model performance is assessed by comparing time series of observed
28 (snow pillow) and modeled snow water equivalent values, by comparing spatially-distributed maps of observed (remotely sensed)
29 and modeled snow depth, and by comparing fieldwork results from within the study area. The results demonstrate that few citizen
30 science measurements are needed to obtain improvements in model performance and these improvements are found in 62% to 78%
31 of the ensemble simulations, depending on the model year. Model estimations of total water volume from a sub-region of the study
32 area also demonstrate improvements in accuracy after CSO measurements have been assimilated. These results suggest that even
33 modest measurement efforts by citizen scientists have the potential to improve efforts to model snowpack processes in high
34 mountain environments, with implications for water resource management and process-based snow modeling.

35 36 **1 Introduction**

37 The importance of snow in ecosystem function, in both human and natural systems, and in water resource management in western
38 North America cannot be overstated (Bales et al., 2006; Mankin et al., 2015; Viviroli et al., 2007). Internationally, more than a
39 billion people live in watersheds where snow is an integral part of the hydrologic system (Barnett et al., 2005). Snowpack dynamics
40 in mountainous, headwater catchments play an essential role connecting atmospheric processes and the hydrologic cycle with



41 downstream water users, agricultural systems, and municipal water systems (Fayad et al., 2017; Holko et al., 2011; Schneider et
42 al., 2013).

43

44 Information about snow distribution comes from many sources. First, there are snow datasets in the form of *in-situ* observations
45 of snowpack conditions, often observations of snow depth or snow water equivalent (SWE). In the United States of America (U.S.),
46 snow depth and SWE data are collected by the National Resources Conservation Service's (NRCS) Snow Telemetry (SNOTEL)
47 network using snow pillows and snow courses. Similar national *in-situ* snow observational networks exist in Europe, like the
48 MeteoSwiss and MeteoFrance programs that include snow depth, snowfall, and SWE datasets. For a comprehensive overview of
49 snow observations in Europe, including each program name, the location of observations, and agency websites, see the European
50 Snow Booklet (Haberkorn et al., 2019). Snow course information is also collected by state programs such as the California
51 Cooperative Snow Survey in the U.S. and, in the case of Canada, by provincial programs such as the British Columbia Snow
52 Survey. These *in-situ* snow observations provide critical information on snow conditions and snow distribution worldwide but vast
53 areas of snowpack remain unsampled.

54

55 To fill the observational gaps associated with point measurements, we often turn to snow information in the form of remote sensing
56 (RS) datasets, like the NASA-based Airborne Snow Observatory (Painter et al., 2016) that uses light detection and ranging
57 (LiDAR) in catchment-scale study areas. Other catchment-scale snow RS datasets are collected using unmanned aerial systems,
58 including high-elevation capable drones and balloon-based platforms in conjunction with structure-from-motion photogrammetry
59 (Buhler et al. 2016; Li et al., 2019). There are also RS datasets covering hemispheric and global scales, like the daily snow covered
60 area product from the MODIS satellite or the GlobSnow snow extent product from the European Space Agency (Hall & Riggs,
61 2016; Luoju et al., 2010).

62

63 Lastly, there are modeled snow datasets, like the Snow Data Assimilation project with a spatial extent that covers large portions of
64 North America (SNODAS; NOHRSC, 2004). There are physically-based snow models that produce snow information on
65 catchment- to hemisphere-scales, like iSnowBal, SnowModel, Alpine3D, PBSM, and SNOWPACK, among many others (Marks
66 et al., 1999; Liston & Elder, 2006a; Lehning et al, 2006; Pomeroy et al., 1993; Lehning et al., 1999). Studies that integrate all of
67 these types of snow information, *in-situ* observations, RS datasets, and process models, are becoming common in snow research
68 because they often produce the best results (Sturm et al., 2015).

69

70 Assimilation of data into process modeling is a strategy that seeks to incorporate measurements of environmental variables into
71 the model chain as a 'hybrid' approach to predicting modeled state variables (Carrassi et al., 2017; Kalnay et al., 2003). There are
72 many examples of data assimilation in the atmospheric sciences and weather prediction (Rabier et al., 2005), in weather reanalysis
73 products (Gelaro et al., 2017; Kalnay et al., 2003; Messinger et al., 2006; Saha et al., 2011), in the hydrological sciences (Han et
74 al., 2012; McLaughlin et al., 2002; McMillan et al., 2013; Park & Xu, 2013), and also in snow science (SNODAS; NOHRSC,
75 2004; Carroll et al., 2001). Data assimilation schemes in snow science rest on the notion that modeled variables like SWE can be
76 merged with an *in-situ* observed value at the same location and time using an objective function. This objective, or cost, function
77 quantifies the differences between the modeled state variable and the observed state (Reichle et al., 2002; Reichle et al., 2008;
78 McLaughlin, 2002). These methods can assimilate model state variables, like SWE, using a statistical method like a Kalman filter
79 or they can assimilate model fluxes like snowfall precipitation or snowmelt rates (Carroll et al., 2001; Clark et al., 2006; Magnussen



80 et al., 2014; Reichle et al., 2008). Other direct insertion assimilation schemes in snow science run the model twice, once without
81 the assimilated data, and a second time after the *in-situ* observations and correction factors are calculated in order to produce an
82 updated state variable (Liston et al., 2008; Malik et al., 2012; Helmert et al., 2018). Regardless of the method of assimilation, the
83 goal is the same: to produce a more accurate modeled state variable (snow depth or SWE) in space and time by using *in-situ*
84 observations to modify the process model output.

85

86 Snow depth measurements are a type of *in-situ* snowpack observation that can be made accurately and quickly by anyone with a
87 measuring device. As a consequence, the current study turns to citizen scientists for snow data collection. Citizen science is a
88 unique type of research in which scientists request input from the general public on data collection, data analysis, or data processing
89 (McKinley et al., 2017; Silvertown, 2009; Wiggins and Crowston, 2011). Through citizen science efforts, researchers access data
90 that are either highly decentralized or concentrated in space, as well as gather measurements frequently or randomly in time. The
91 primary advantage is that many people can accomplish data collection at spatial and temporal scales well beyond the capacity of a
92 single researcher or small group of scientists (Bonney et al., 2009; Cooper et al., 2007; Dickinson et al., 2010). Recent successful
93 citizen science-based research includes the CrowdHydrology project that monitors stage heights of streams and rivers (Fienen &
94 Lowry, 2012; Lowry & Fienen, 2013), and the CrowdWater project, which obtains multiple types of crowdsourced measurements
95 of hydrological variables using a publicly available app (Seibert et al., 2019; van Meerveld et al., 2017). Buytaert et al. (2014)
96 provides a comprehensive review of the recent challenges and motivations of citizen science in hydrology. This unique type of
97 data collected by citizen scientists has been used in many natural sciences, and snow hydrology represents a new opportunity for
98 citizen science-based research.

99

100 The present study explores the assimilation of a unique type of citizen science-based data in snow modeling: snow depth
101 measurements collected by citizen scientists traveling in snow covered landscapes worldwide. This new snow dataset and project
102 is called Community Snow Observations (CSO; communitysnowobs.org). The CSO campaign relies on backcountry recreationists
103 including skiers, snowboarders, snowmachiners, cross country skiers, snowshoers, and snow professionals, including avalanche
104 forecasters and snow scientists, who visit snowy environments for work and recreation to obtain snow depth measurements of the
105 snowpack (Hill et al., 2018; Yeeles, 2018). Other citizen science projects are underway in snow science, including research on the
106 relationship between vernal windows and snow depth (Contosta et al., 2017; Burakowski et al., 2018), snow depth verification of
107 satellite datasets in Canada using Twitter (Edmiston, 2012; Wiggins & Crowston, 2011), and the backyard precipitation
108 measurement campaign called Community Collaborative Rain, Hail, and Snow Network (Reges et al., 2016). The CSO project
109 adds to a growing body of research accomplished by citizen scientists in the natural sciences, and contributes to the connections
110 between physics-based, process modeling and *in-situ* observations in data assimilation and snow science.

111

112 The current study aims to answer two questions. First, can citizen scientists' snow depth measurements be incorporated into the
113 process model workflow in a way that improves model performance? This question is addressed by presenting an ensemble of
114 modeled snow depth and SWE distribution results with two types of outputs: (a) a set of model outputs without any snow depth
115 measurements assimilated and, (b) a set of model outputs with CSO snow depth measurements assimilated. To answer this first
116 question, we characterize the results using temporal and spatial datasets for validation. These datasets include time-series SWE
117 observations at a SNOTEL station in the study area and lidar- and photogrammetry-derived snow depth maps from 2017 and 2018.
118 We rely upon common metrics for characterizing the spatial distribution of modeled versus observed continuous environmental



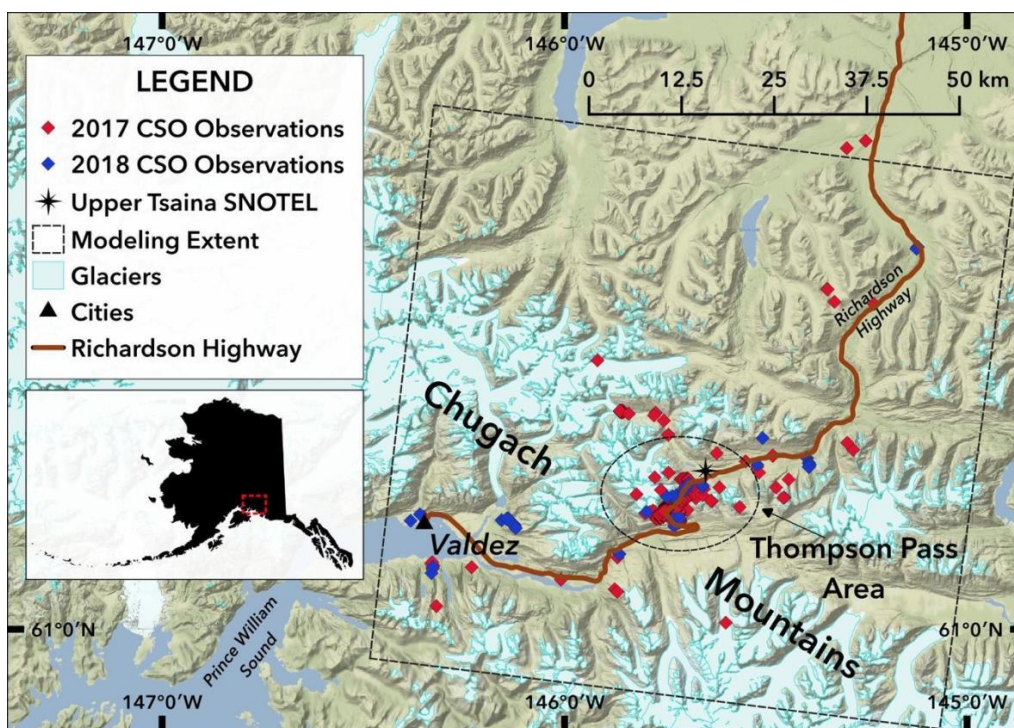
119 variables to assess the value of the CSO modified outputs (Reimann et al., 2010). Secondly, how do the results vary with the
120 number of the CSO measurements assimilated? We address this question by randomly selecting and varying the quantity of CSO
121 measurements in the ensemble members. The potential of mobilizing a new type of *in-situ* snow dataset collected by snow
122 professionals and snow recreationists is significant because these participants often travel to remote mountainous environments
123 worldwide where *in-situ* snow observations are sparse.

124

125 **2 Study Area**

126 The study focuses on a 5,736 km² area of the eastern Chugach Mountains near Valdez, Alaska (Figure 1). This high-relief, glacier-
127 carved landscape ranges from sea-level in Port Valdez to rugged peaks exceeding 2200 m.a.s.l., and a mountain pass on the
128 Richardson Highway, named Thompson Pass (815 m.a.s.l). This region of the Chugach mountains receives extreme amounts of
129 snowfall, with Thompson Pass holding multiple snowfall records for the state of Alaska, including the 1-day total (1.57 m), 2-day
130 total (3.06 m), and weekly total (4.75 m; Shulski & Wendler, 2007). Like other places in the Chugach Mountains, snow densities
131 and snow depths in the region vary greatly across short distances (Wagner, 2012). There are deep, dense, and wet snowpacks found
132 in the maritime snow climates near the coast. The interior regions of the Chugach Mountains further from the coast contain
133 shallower, less-dense, and drier snow climates (Fieldwork 2018; Sturm et al., 1995; Sturm et al., 2010). These factors are important
134 because the Thompson Pass region and the Chugach mountains are frequently accessed by backcountry skiers and snowboarders,
135 backcountry snowmachiners, and multiple heli-skiing operations due to the exceptional access to steep terrain, and deep, mountain
136 snowpack (Carter et al., 2006; Hendrikx et al., 2016). Due to the popularity of the area for backcountry snowsports and the risk of
137 danger for avalanches affecting highway conditions, the Valdez Avalanche Center produces avalanche forecasts for many of the
138 slopes adjacent to the Richardson Highway in the Thompson Pass region. The choice of a study area within a mountainous region
139 visited regularly by snow recreationists and professionals is essential for the present study. For these reasons, the Thompson Pass
140 region of the Chugach Mountains in Alaska was selected for the initial phases of the CSO project.

141



142
143
144
145

Figure 1: Study Area Map.
The study area maps showing the Community Snow Observations (CSO) measurements, the modeling spatial extent, and the Thompson Pass region of the Chugach Mountains.

146 3 Methods and Datasets

147 3.1 Model Dataflow

148 This study relies on a common research design in snow science that uses (1) *in-situ* snow observations, (2) physically-based process
149 modelling, and (3) remote sensing of the snowpack to accomplish its primary objectives (Sturm et al., 2015). Figure 2 is a
150 conceptual diagram of how the citizen scientists' snow depth measurements fit into the model chain for the present study. The
151 modeling process begins with the weather forcing products and citizen scientists' snow depth observations as model inputs. Sub-
152 models for meteorological variable distribution, snow depth to SWE estimation, and for the assimilation of snow measurements
153 are employed before the final simulation occurs. The process model outputs are then validated by the RS datasets, the UTS station
154 record, and the 2018 field measurements. Incorporating the citizen scientists' observations into the model chain is an attempt to
155 modify the model outputs by *in-situ* snow depth observations.

156

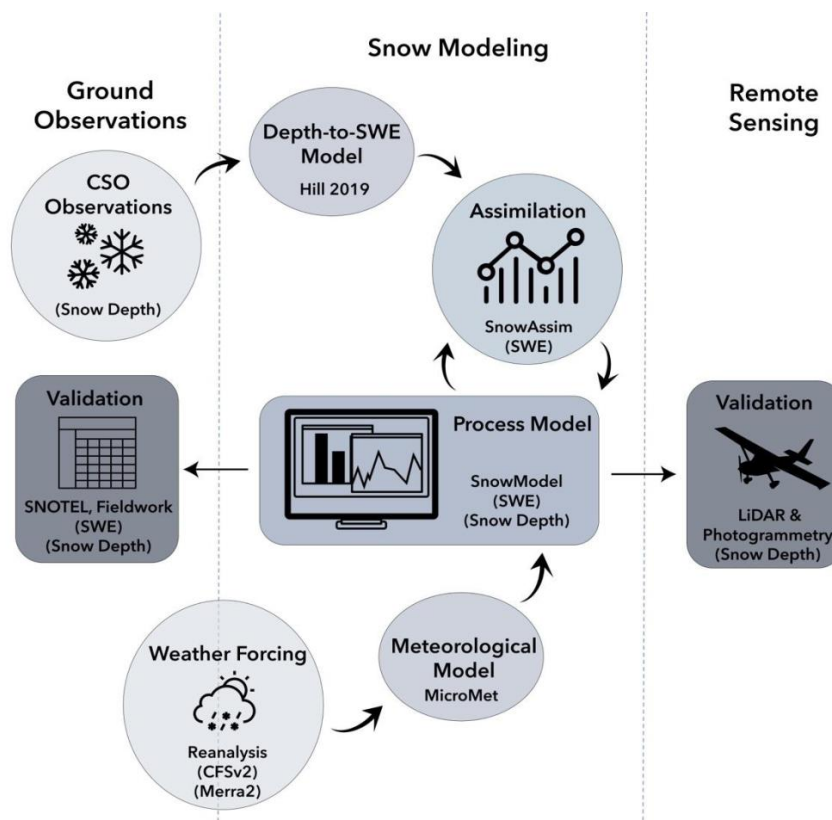


Figure 2: Model Dataflow Diagram.

The model chain begins with the weather forcing product and the Community Snow Observations (CSO) datasets. The arrows indicate dataflow through the series of sub-models to the process model output. The model output is then validated by the SNOTEL station time-series, the 2018 fieldwork, and the remote sensing datasets.

157

158

159

160

161

162

163 3.2 Modeling Framework

164 In this study we used a sequence of models to simulate SWE and snow depth distributions within the Thompson Pass study area
165 during WY2017 and WY2018. The sections below provide brief information about the models used in this study. For more details,
166 please refer to the source citations for each model.

167

168 3.2.1 SnowModel

169 SnowModel (Liston & Elder, 2006a) is a physically-based, spatially distributed process model for simulating the evolution of
170 snowpacks in snowy environments, and has been used for high-resolution and hemispheric-scale modeling worldwide (Beamer et
171 al., 2016; Beamer et al., 2017; Crumley et al., 2019; Liston & Heimstra, 2011; Mernild et al., 2017a-b). SnowModel is chosen for
172 the Chugach Mountains study area since it contains a data assimilation sub-model, SnowAssim, and a snow transportation sub-
173 model, SnowTran3d. Within SnowModel, various other sub-models solve the energy budget for the snowpack, generate runoff



174 quantities, etc. The present study focuses on the snow depth and SWE distribution outputs from SnowModel from simulations with
175 and without the data assimilation sub-model.

176

177 **3.2.2 MicroMet**

178 MicroMet (Liston & Elder, 2006b) is a meteorological distribution sub-model for weather station or reanalysis datasets that can be
179 paired with SnowModel in spatially explicit modeling applications. MicroMet uses the Barnes objective analysis scheme for
180 interpolating meteorological input variables to the gridded SnowModel domain for each model timestep (Barnes, 1964; Barnes,
181 1973). In the present study, instead of using weather station data, the model is forced with reanalysis data and MicroMet uses the
182 node locations as weather stations, accessing the reanalysis node surface level precipitation, wind speed and wind direction, relative
183 humidity, air temperature, and elevation variables for the spatial interpolation. MicroMet has been paired with reanalysis weather
184 products and SnowModel in many studies worldwide (Baha et al., 2018; Beamer et al., 2016; Liston & Heimstra, 2011; Mernild
185 et al., 2017a).

186

187 **3.2.3 SnowTran3d**

188 Wind redistribution of snow is an important factor for the spatial distribution of snow depths and SWE distributions for snow
189 modeling (Clark et al., 2011). Wind events build snow deposits in the gullies and the leeward side of bedrock features into drift
190 depths greater than 10 m at times within the Thompson Pass study area. These events also leave some portions of the landscape
191 completely scoured and void of snow based on fieldwork observations and the RS snow surveys from both years. SnowTran3d is
192 a sub-model within SnowModel that redistributes the snow laterally in the model grid according to the processes that govern snow
193 transportation: fetch, wind speed, wind direction, wind shear stress and the shear strength of the snowpack, saltation and turbulent
194 suspension of the snow, and sublimation (Liston et al., 2007). SnowTran3d is suitable for use as a sub-routine within SnowModel
195 when the model grid cell resolution is appropriate for the length scale of snow transportation processes to occur, for example,
196 primarily at model resolutions less than 100 m.

197

198 **3.2.4 SnowAssim**

199 To assimilate the CSO measurements, we used the sub-model SnowAssim developed in tandem with SnowModel (Liston and
200 Elder, 2008). For each water year (WY; defined as September 1st through August 31st) in the model time period, SnowModel
201 creates a full, preliminary simulation using the meteorological forcing dataset and no observational SWE data. Next, SnowAssim
202 compares the observed state SWE values at each location and time to the modelled state SWE values from the same grid locations
203 and time iterations. Note that CSO measurements are submitted as snow depths (m) and SnowAssim requires observational inputs
204 to be SWE depths (m), so a conversion from depth to SWE was necessary. The snow depth to SWE conversion method for the
205 current study will be discussed in the following section. SnowAssim aggregates all the assimilated observations by date and creates
206 a spatially varying correction surface that covers the entire model domain (Liston and Elder, 2008). These various correction
207 surfaces are applied by adjusting the model precipitation fluxes and snowmelt factors between SWE observation dates during a
208 second SnowModel simulation.



209

210 **3.2.5 Snow Depth to Snow Water Equivalent Conversion**

211 CSO participants take measurements of snow depth yet SnowAssim requires SWE observation inputs. A conversion from snow
212 depth to SWE must be performed. A body of research exists on the best methods for converting point measurements from snow
213 depth to SWE, using either bulk density estimations, snow climate classifications, statistical models, or atmospheric conditions
214 and energy balance approaches (Sturm et al., 1995; Sturm et al., 2010; McCreight and Small 2014; Jonas et al., 2009; Pagano et
215 al., 2009; Hill et al., 2019; Pistocchi, 2016). The Hill et al. (2019) model was chosen for two reasons. First, the data requirements
216 are minimal for this model, requiring only location, day of water year (DOY) and readily-available climatological information
217 based on input location. These minimal requirements align with the information available from CSO measurements. Second, it
218 was found to outperform other bulk density methods such as Sturm et al. (2010) and Jonas et al. (2009) when tested against a wide
219 variety of snow pillow and snow course datasets (Hill et al., 2019).

220

221 **3.3 Model Input Datasets**

222 **3.3.1 Elevation and Land Cover**

223 SnowModel requires a digital elevation model (DEM) and a land cover model as two of the three primary input datasets. The DEM
224 is the National Elevation Dataset (NED) from the United State Geological Survey downloaded at 30 m resolution and then rescaled
225 to 100 m spatial resolution (Gesch et al., 2002). The land cover model is the National Land Cover Database (NLCD) 2011 dataset
226 at 30 m spatial resolution and then also resampled to 100 m resolution (Homer et al., 2011). The NLCD dataset is also reclassified
227 to match the land cover input classes required by SnowModel. Initially, we test results from model simulations at two spatial
228 resolutions, 30 m and 100 m, covering the model domain in the Thompson Pass region of the Chugach mountains. After calibrating
229 the model, the results section only includes the 30m resolution.

230

231 **3.3.2 Weather Forcing Datasets**

232 Various weather reanalysis products have been used in remote portions of Alaska in previous studies (Beamer et al., 2016; Beamer
233 et al., 2017; Crumley et al., 2019; Liston & Heimstra, 2011). In Alaska, each reanalysis product shows bias corresponding to
234 meteorological variable, regional location, and season of the year (Lader et al., 2016; see their Figures 3 and 4). For this reason,
235 the current study considered two weather reanalysis products that differ in their biases in temperature and precipitation in the
236 Thompson Pass region during the winter and the summer seasons. We used the Climate Forecast System Reanalysis version 2
237 product (CFSv2) and the Modern-Era Retrospective Analysis for Research and Applications version 2 (MERRA2) product for the
238 weather forcing inputs for SnowModel. The CFSv2 product from the National Centers for Environmental Prediction is an extension
239 of the Climate Forecast System Reanalysis (CFSR) version 1 product that began in 1979, albeit at a lower spatial resolution (Saha
240 et al., 2010). The CFSv2 data are available at a spatial resolution of 0.2 arc degrees, and a 6 hr temporal resolution (Saha et al.,
241 2014). This CFSv2 dataset was downloaded using Google Earth Engine (GEE), a platform for accessing and analyzing scientific
242 datasets with global coverage. The MERRA2 weather reanalysis product from NASA's Global Modeling and Assimilation office
243 is the second meteorological forcing dataset tested in the present study (Gelaro et al., 2017). The MERRA2 data are available at a



244 spatial resolution of 0.667 degrees by 0.5 degrees, with a 3 hr temporal resolution beginning in 1979. MERRA2 replaces the older
245 version product with updated assimilation processes to include more weather datasets.

246

247 **3.4 Snow Datasets**

248 **3.4.1 Snow Telemetry Station Data**

249 The study area contains two SNOTEL stations operated by NRCS. The first station is the Upper Tsaina SNOTEL (UTS) station
250 located at 534 m.a.s.l. on the NE side of Thompson Pass reporting the full standard set of sensor variables, including precipitation,
251 temperature, snow depth, and SWE. The second station is the Sugarloaf Mountain SNOTEL (SLS) station, located near the Valdez
252 Arm of the Prince William Sound at 168 m a.s.l. in the SW corner of the study area and records only precipitation, temperature,
253 and snow depth, but not SWE (Figure 1). Detailed information about the SNOTEL sensors and climate monitoring instruments
254 can be found at the SNOTEL website (<https://www.wcc.nrcs.usda.gov/snow/>) and Serreze et al. (1999). Direct links to the
255 SNOTEL websites for the UTS and SLS stations can also be found in the Data Availability section below.

256

257 **3.4.2 LiDAR and Photogrammetry Derived Data**

258 The airborne photogrammetry survey was conducted on April 29, 2017 with a Nikon D800 36.2 megapixel camera and flown on
259 a fixed-wing aircraft above a portion of the Thompson Pass study area, see Figure 3 for location and extent. An onboard Trimble
260 Global Navigation Satellite System (GNSS) and a base-station were used for positional control. Post-processing was completed
261 with structure-from-motion software to create a digital surface model (DSM) of the photogrammetry-derived snow surface. The
262 airborne LiDAR survey was collected on April 7th and 8th, 2018, using a Riegl VUX1-LR laser scanner flown on a fixed-wing
263 aircraft. An onboard integrated inertial measurement unit (IMU) and GNSS, and a base-station were used to provide positional
264 control for the LiDAR-derived snow DSM. Both RS datasets were evaluated against a previously collected photogrammetry-
265 derived DSM from 2014 when no snow was present. An interpolation scheme was used to gap-fill some of the negative values in
266 the snow DSM due to vegetation cover effects.

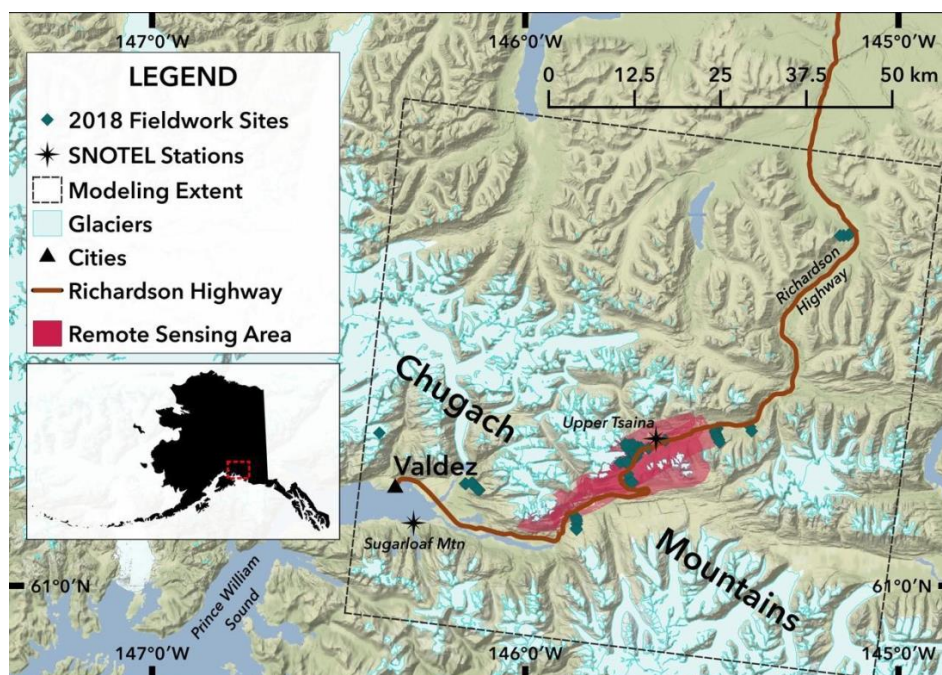
267

268 **3.4.3 Chugach 2018 Fieldwork Data**

269 Three weeks of fieldwork in the Thompson Pass region were conducted in March, April, and May of 2018. Snow depth and SWE
270 were measured throughout the study area with an avalanche probe and a Federal Snow Sampler. At each fieldwork measuring site,
271 a central SWE measurement was taken using the Federal Sampler. Avalanche probes were used in the surrounding 100 m² to take
272 a series of 8 snow depth measurements extending 5 m in each direction from the central SWE measurement. The fieldwork
273 sampling protocol was designed to consider: (1) variability in snow depth in small areas less than 100 m², (2) month-to-month
274 changes in snow depth and SWE, and (3) spatial gradients in snow density throughout the entire study area. A diagram of the
275 location of each observational site can be found in Figure 3. The 2018 fieldwork dataset was used for validation with two purposes
276 in mind. First, the 2018 fieldwork SWE measurements were used as a validation dataset for the 2018 SWE distribution results.
277 Secondly, since the data collected in the spring of 2018 contains measured snow depths and SWE at 70 observational sites (n =



278 560; 8 per site), we conducted an analysis of the sub-grid scale variability in snow depth found at each observational site and these
279 results are found in the discussion section.
280



281
282
283
284
285

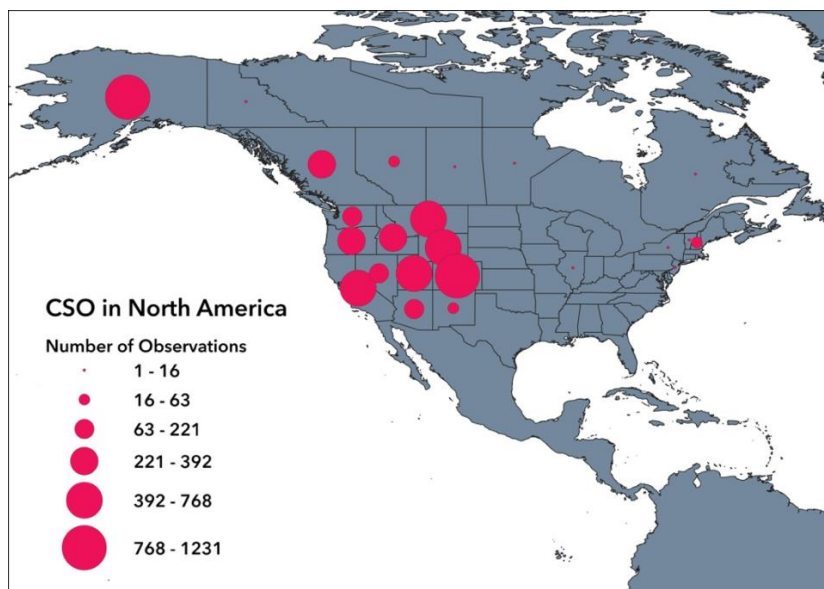
Figure 3: Validation Datasets Map.
The 2018 fieldwork includes 72 sites with co-located snow water equivalent and snow depth measurements. The remote sensing datasets from 2017 and 2018 are overlain on the map, along with the location of the Upper Tsaina SNOTEL station.

286 3.4.4 Community Snow Observations Data

287 The CSO program collects snow depth data from citizen scientists in snowy environments worldwide. Full details including links
288 to smartphone apps and tutorials are found at <http://communitysnowobs.org>. Citizen scientists take several (2 to 4) snow depth
289 measurements within a small area (< 4 m²) using an avalanche probe or other depth measuring device (meterstick, etc.). These
290 measurements are then averaged by the participant and submitted using the app or program preferred by the participant. The
291 submitted data include the global positioning system (GPS) location in latitude and longitude, time and date, and snow depth
292 measurement (cm). The accuracy of the GPS system for each participants' mobile device determines the location error of the GPS,
293 with common errors for mobile phones ranging between +/- 4 to 7 m (Garnett & Stewart, 2015; Schaefer & Woodyer, 2015). Since
294 the model resolution is 30 m and 100 m, this level of horizontal error in GPS location is acceptable for the purposes of our research
295 questions. All collected data are made freely available on the CSO website for visualization and download (see Section 9 for Data
296 Availability). Thousands of measurements have been recorded by participants in CSO globally since it began in January 2017 with
297 initial measurement campaigns in Alaska and other frequently visited locations in mountain regions across North America (Figure
298 4). In the modeling domain of the current study, 442 CSO measurements were available for WY2017 and 104 CSO measurements



299 for WY2018. These measurements were concentrated in the Thompson Pass region of the study area (Figure 1) and range from 25
300 m to 1400 m in elevation.
301



302
303
304
305
306

Figure 4: CSO Participation in North America.
Participation in the Community Snow Observations (CSO) project in North America aggregated by the number of observations recorded in each U.S. state or Canadian province between January 1st, 2017 and December 31st, 2019.

307 4 Calibration

308 We performed model calibration using five years of the historical record of the UTS station from WY2012 through the end of
309 WY2016. The calibration was focused on adjustments to temperature lapse rates, precipitation lapse rates, wind adjustment factors,
310 and use of the SnowTran3d sub-model. We chose temperature lapse rates and precipitation lapse rates for calibration because
311 SnowModel is known to be limited by these factors when large elevational differences exist within the model domain (Liston and
312 Elder, 2006). We chose wind adjustment factors and the wind transportation sub-model for calibration because wind redistribution
313 of snow plays a significant role in the study area based on the 2018 fieldwork and the RS surveys from 2017 and 2018. Since the
314 SnowAssim sub-model requires a single layer snowpack, no adjustments were made to the snowpack layer structure. For each
315 weather reanalysis product a full calibration was performed for the 30m and 100m model resolutions, in the event that spatial
316 resolution plays a significant role in parameter selection. See Appendix A for the descriptions of the model parameters tested
317 during the calibration.

318

319 The daily SWE output from each calibration simulation is compared with the UTS observed SWE for the duration of the 5-year
320 calibration time period using root mean squared error (RMSE), the Nash Sutcliffe Efficiency (NSE), the Kling-Gupta Efficiency
321 (KGE), and mean bias error (Bias) to assess the calibration simulations. Table 1 lists the best 30m and 100m calibration simulations,
322 based on their time-series RMSE, NSE, KGE, and Bias scores. We acknowledge that measurement errors can occur with SNOTEL



323 snow pillows and that these well known errors may affect the accuracy of the observational dataset (Johnson and Schaeffer, 2002;
324 Johnson, 2004).

325

326

327

328

Table 1: Model Calibration Results.
The best calibration results are given for each set of simulations for water years 2012-2016, along with the root mean squared error (RMSE), the Nash Sutcliffe Efficiency (NSE), the Kling-Gupta Efficiency (KGE), and the mean bias error (Bias).

Reanalysis Product & Resolution	Time Step	Number of Simulations	RMSE SWE (cm)	NSE	KGE	Bias SWE (+/- cm)
MERRA2, 30m	3hrly	45	24	-0.29	0.08	+16
MERRA2, 100m	3hrly	45	26	-0.10	-0.10	+19
CFSv2, 30m	6hrly	45	22	-0.15	-0.01	+17
CFSv2, 100m	6hrly	45	22	-0.15	-0.01	+17

329

330 Calibration results in Table 1 show that the 30m model grid resolution slightly outperforms the 100m model grid resolution in the
331 MERRA2-forced calibration simulations. However, the CFSv2-forced simulations show no difference between the model grid
332 resolutions. The CFSv2 product slightly outperforms the MERRA2 product in terms of SWE RMSE. Overall, the differences
333 between the top performing model grid resolution and reanalysis product are mixed and potentially negligible, varying by metric.
334 The NSE and KGE model performance metrics in the calibration simulations are lower than expected, due primarily to precipitation
335 inputs from the reanalysis products that were consistently higher than measured precipitation at the UTS station. Since SnowAssim
336 adjusts the precipitation fields during assimilation, these input deficiencies are acceptable for the purposes of this study. The
337 SnowModel default parameter values notably and consistently produce the top performing simulations, see Appendix B for details.
338 Due to each of these factors, the calibrated model for the remainder of the study uses the CFSv2 reanalysis product, the 30m model
339 grid resolution, and the SnowModel default parameter values.

340

341 One of the primary obstacles for process modeling is the use of accurate weather input data, and the related uncertainties with
342 weather inputs are a well-known complication in snow and hydrological modelling (Rivington et al., 2005; Schmucki et al., 2013;
343 Schlogl et al., 2016). Initial tests of modeled precipitation fields using Micromet versus the observed precipitation at the UTS
344 station revealed that both reanalysis products overestimated the amount of precipitation observed in the study area at the UTS
345 station. With these obstacles in mind, we designed an experiment to supplement the main findings of this research. For this
346 experiment we introduced a model precipitation adjustment factor similar to the method outlined in Mernild et al. (2006). We
347 applied this scalar value to the precipitation fields as a bias correction of the precipitation inputs. We tested 11 precipitation
348 adjustment factors ranging from 0.95 to 0.45 and applied them to the meteorological forcing inputs during the 5-year calibration
349 time period. For more details about the precipitation adjustment factor results, see Appendix C. This experiment, presented in
350 section 6.5, allows us test improvements to model performance when the precipitation inputs are bias corrected prior to model
351 assimilation of CSO measurements.

352



353 **5 Experimental Design**

354 With the model calibrated, we carried out a series of simulations in order to (1) quantify the improvement in model performance
355 due to the assimilation of CSO measurements and to (2) understand the effects of the number of CSO data points selected for
356 assimilation. Model simulations without using CSO measurements provide a baseline for comparison, referred to as the NoAssim
357 case. Ensemble model simulations were also carried out with various numbers of CSO measurements assimilated, referred to as
358 the CSO simulation case. An ensemble of 60 trials per year were carried out with $n = 1$, $n = 2$, $n = 4$, $n = 8$, $n = 16$, and $n = 32$,
359 where n equals the number of CSO measurements assimilated per WY. In each instance (n value), 10 realizations of the numerical
360 experiment were carried out.

361

362 The timeframe of the assimilating CSO measurements was restricted to the peak SWE period or later. According to the UTS station,
363 peak SWE in the study area generally occurs mid- to late-April and consequently the earliest assimilation date was set to April
364 15th. The CSO measurements were aggregated by week because initial simulations suggested that daily increments were not
365 producing realistic results by SnowAssim. Additionally, CSO participation in the Thompson Pass region during the early
366 accumulation season was infrequent in WY2018 and non-existent in WY2017. Since peak SWE is important for mountain
367 hydrology and ecology, with many snow studies using it as an indicator metric, the time restrictions are acceptable for the research
368 questions addressed in this study (Bohr and Aguado, 2001; Trujillo et al., 2012; Kapnick and Hall, 2012; Mote et al., 2018;
369 Wrzesien et al., 2017).

370

371 **6 Results**

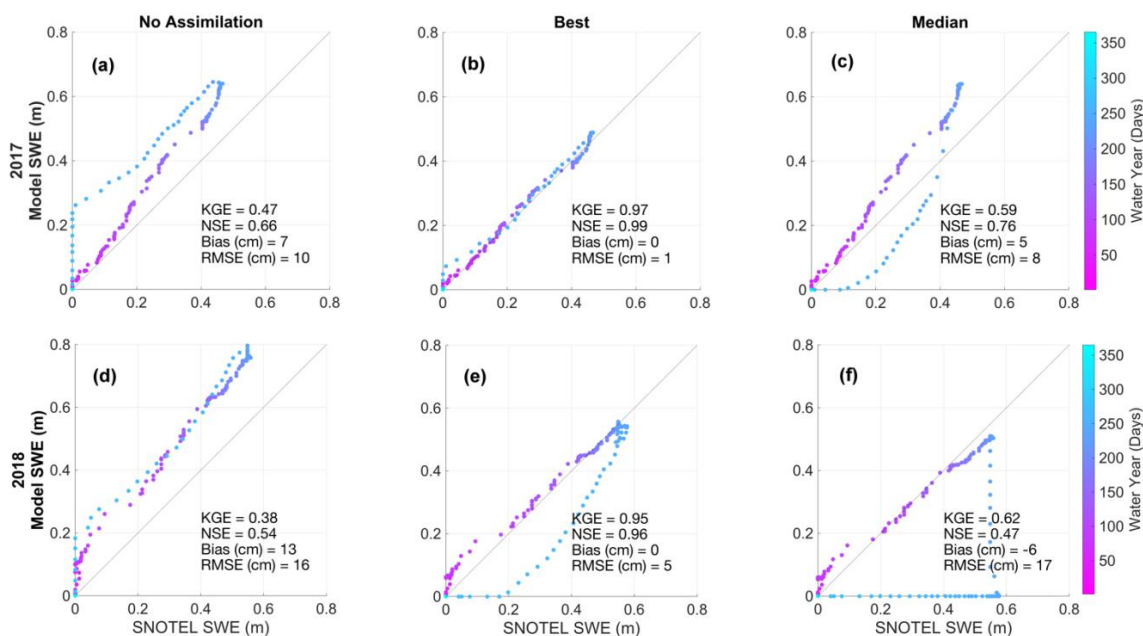
372 The following results reflect the three types of available validation datasets: 1) time-series SWE results at the UTS station, 2)
373 spatial snow depth distributions from the RS datasets, and 3) point-based snow depth and SWE measurements from the 2018
374 fieldwork.

375

376 **6.1 Temporal Results Using the Upper Tsaina SNOTEL Station**

377 The temporal results compare the UTS station SWE time-series to the ensemble member SWE time-series during WY2017 and
378 WY2018. Figure 5 displays the temporal cycle of snowpack accumulation and ablation, and the timing of peak SWE. At the UTS
379 station in the study area, the average WY day of peak SWE is 228, or April 15th. Before this day, the snowpack is generally
380 increasing in SWE and afterwards the snowpack generally enters the ablation period with a reduction in SWE. This temporal cycle
381 can be observed in Figure 5 by following the color gradient. The highest performing (Best) CSO simulation (Figure 5b,e) corrects
382 the slope of the snowpack accumulation and ablation phases when contrasted with the NoAssim accumulation and ablation phases
383 and slopes (Figure 5a,d). These time-series results, in terms of model performance metrics and the snowpack temporal cycle,
384 exhibit SnowAssim's ability to incorporate CSO measurements and improve modeled SWE outputs at the UTS station location
385 throughout the entire snow season.

386



387

388

389 **Figure 5: Time Series at Upper Tsaina SNOTEL Station.**
390 **The Upper Tsaina SNOTEL snow water equivalent (SWE) observations versus the modeled SWE for the no assimilation case (a,d), the**
391 **Best CSO simulation (b,e), and the Median CSO simulation (c,f). The timeseries color gradient corresponds to the day of the water**
392 **year.**

392

393 Figure 5 summarizes the temporal results for the Best and median performing (Median) CSO simulations, including the NoAssim
394 case. Each ensemble member is evaluated by their KGE, NSE, RMSE, and Bias scores. For results presented in this section, the
395 KGE score is used to rank the ensemble simulations. A full accounting of each ensemble member and their time-series ranking can
396 be found in Appendix D. Modeled SWE depths for the NoAssim case are consistently higher than the UTS station SWE
397 observations for both WYs (Figure 5a,d). The modeled SWE depths for the Best CSO simulation outperform the NoAssim case
398 throughout the entirety of the time-series and represent an improvement in model performance scores according to all of the time-
399 series metrics (Figure 5b,e). The modeled SWE depths for the Median CSO simulation for WY2017 outperform the NoAssim case
400 by all metrics, and the WY2018 Median CSO results are mixed. The ensemble simulation KGE scores outperform the NoAssim
401 KGE scores among 70% of the WY2017 ensemble members, and among 67% of the WY2018 ensemble members. Any number
402 of CSO measurements assimilated show improvements in model performance, a key finding in the time-series results.

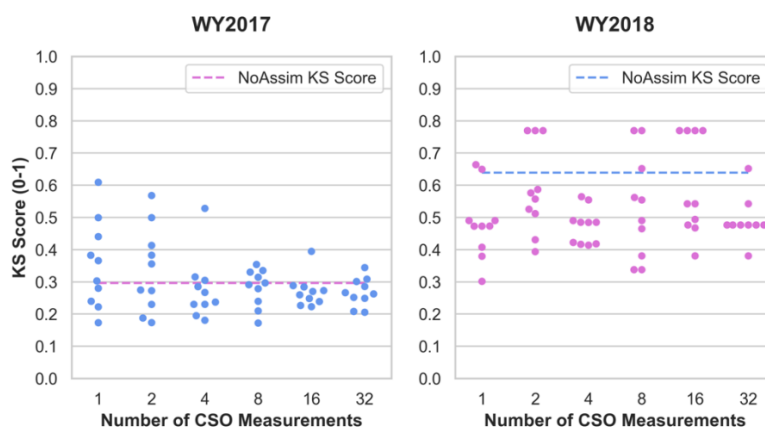
403

404 6.2 Spatial Results Using the Remote Sensing Datasets

405 The ensemble results are summarized in Figure 6 using the Kolmogorov-Smirnov statistic (KS; Massey 1951). The KS statistic
406 quantifies the difference between a reference dataset of a continuous variable and a sample dataset of the same variable. The KS
407 statistic represents the maximum distance between the empirical cumulative distribution function (ECDF) of the reference and
408 sample datasets, with KS scores ranging from zero to one, with zero representing perfect dataset agreement (Reimann et al., 2010).
409 In the KS analysis, the reference dataset is the RS derived snow depth distribution and the sample datasets are each of the ensemble



410 snow depth distributions, including the NoAssim case. Figure 6 shows that in WY2017 the CSO simulations are an improvement
411 from the 2017 NoAssim case among 62% of the ensemble members, and in WY2018 among 78% of the ensemble members. Note
412 that only the KS values that fall below the NoAssim line represent an improvement in model performance during the CSO
413 simulations. The spatial results reveal that improvements in model performance are not dependent upon the number of CSO
414 measurements that are assimilated in WY2018. However, WY2017 has a smaller range in KS values as the number of assimilated
415 measurements increases, with more CSO simulations outperforming the NoAssim case. These results also vary according to model
416 performance metric and by WY, with no clear pattern emerging from the number of measurements assimilated.
417



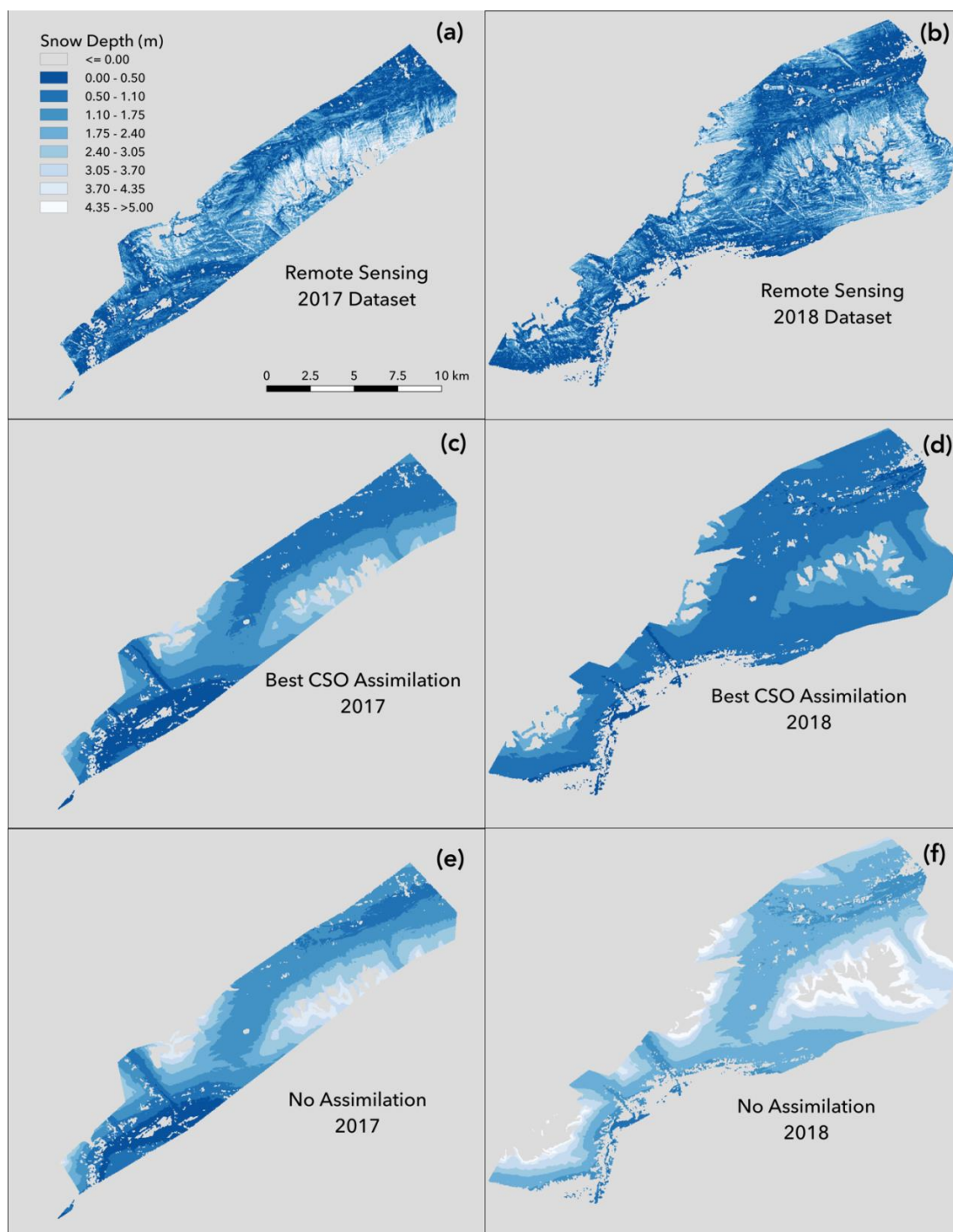
418
419
420
421

Figure 6: Swarmplots of Kolmogorov-Smirnov Scores.
The ensemble simulations are ranked by Kolmogorov-Smirnov (KS) score per year and plotted according to the number of measurements assimilated, including the no assimilation (NoAssim) case.

422

423 The snow depth distribution maps in Figure 7 display the RS datasets (a,b), the results from the highest performing CSO simulation
424 (c,d), and the NoAssim case for each WY (e,f). Refer to Figure 2 for the RS dataset location within the study area. We present the
425 Best CSO simulation as the focus of Section 6.2 ranked according to KS score ranking (Figure 6). A full accounting of each
426 ensemble member and their spatial distribution ranking can be found in Appendix E. In the RS datasets, there is more variation
427 and heterogeneity in snow depth across short distances (Figure 7a-b). This spatial diversity is evident even after the RS dataset has
428 been aggregated to correspond to the model resolution at 30 m, as depicted in Figure 7. The NoAssim case and Best CSO simulation
429 show less spatial diversity, and the NoAssim case broadly overestimates snow depth when compared to the Best CSO simulation
430 for both WYs. The visualization of the snow depth distributions in Figure 7 illustrate the challenges of accurately representing the
431 process scale through physics-based modeling at low resolutions (Blöschl 1999), and some of these challenges will be examined
432 further in the discussion section.

433
434



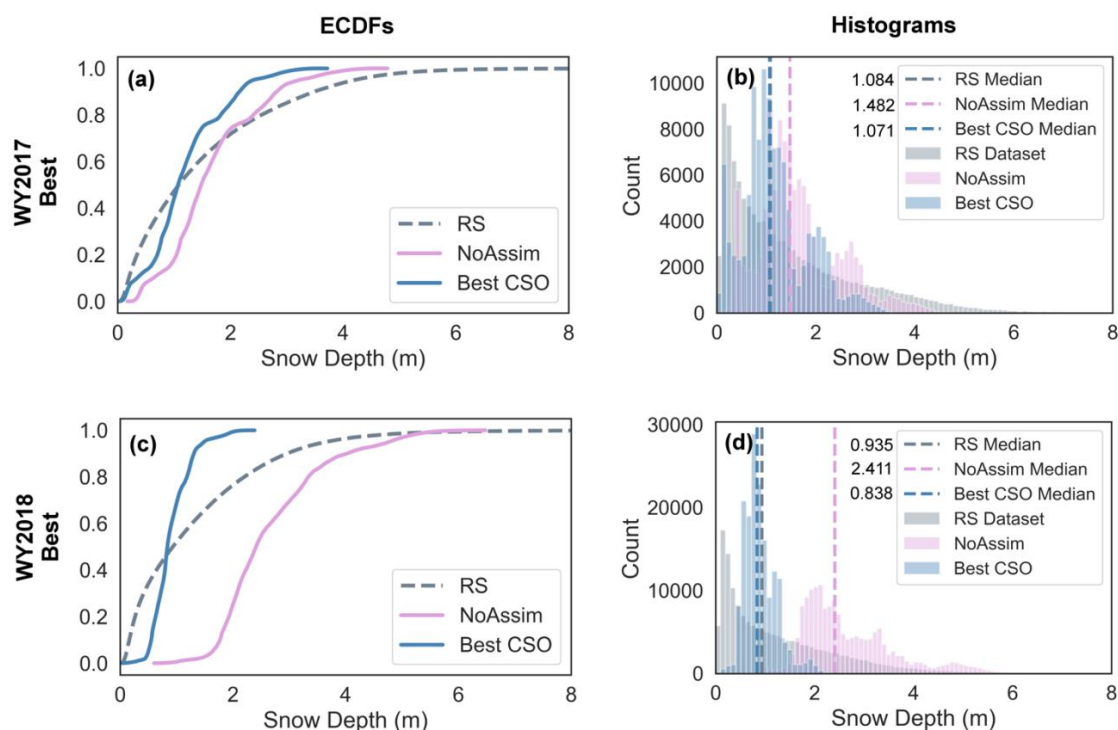
435
436
437
438
439

Figure 7: Snow Depth Distribution Maps.
(a,b) The remote sensing (RS) datasets from 2017 and 2018. (c,d) The best CSO simulation results corresponding to the RS dataset spatial extent. (e,f) The no assimilation results corresponding to the RS dataset spatial extent. The total model area that corresponds to the RS dataset in 2017 is 104 km² and 149 km² in 2018.



440

441 Figure 8 presents histograms and empirical cumulative distribution functions (ECDFs) for the RS datasets, the NoAssim case, and
442 the Best CSO simulation. In WY2017 (Figure 8a), when the NoAssim case overestimates snow depths, the Best CSO simulation
443 ECDF shifts left, towards the RS dataset ECDF. To a greater degree, in WY2018 (Figure 8c) when the NoAssim case more broadly
444 overestimates the snow depths, the Best CSO simulation ECDF shifts further left, towards the RS dataset ECDF. The shifts in the
445 ECDFs are evident in the histograms and the median value of each dataset is indicated with a dashed line (Figure 8b,d). The same
446 shifts are evident in the snow depth distribution maps (Figure 7c,d,e,f). Even though the shifts in ECDFs and histograms are in the
447 correct direction in the Best CSO simulations, SnowAssim is not adjusting the distribution of snow depth values, which can be
448 seen in the multimodal shape of the histograms.
449



450

451

452

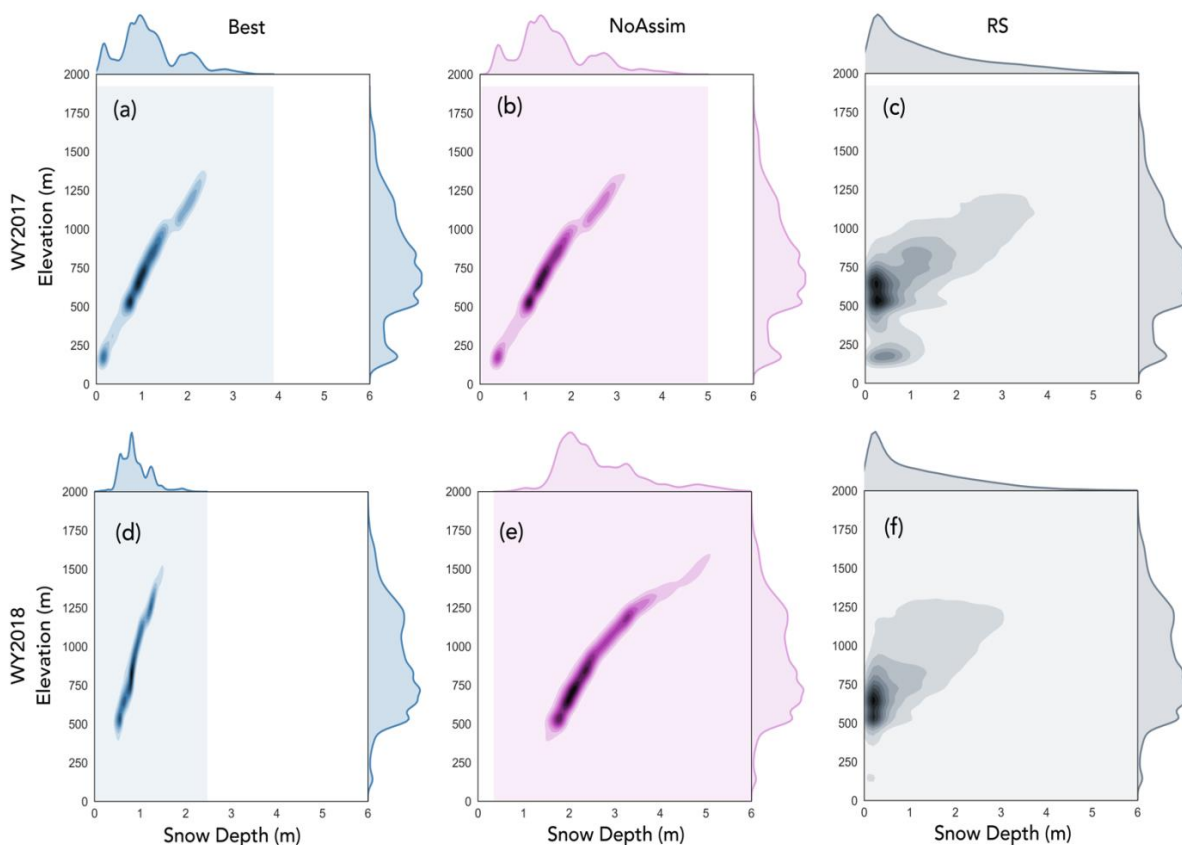
453

454

455 The multimodal distribution of snow depths in the modeled results can be explained by their relationship to the elevation of the
456 surrounding terrain. The input DEM and the snow depth distributions were compared on a grid-cell-to-grid-cell basis using a two-
457 dimensional histogram (2DH). Figure 9 is a series of 2DHs that display snow depth (x axes) versus the input DEM (y axes) in the
458 RS area from both years. Darker colors indicate a higher frequency of snow depth and elevation values corresponding to each
459 dataset. The 2DHs show a proportional relationship between the modeled snow depths (Figure 9 a,b,e,f) and the input DEM values.
460 As elevation increases, snow depth also increases linearly in the modeled results. Still, the range of snow depths from Best CSO



461 simulation shifts towards the RS dataset in both years, but the elevation relationship remains largely intact. The RS snow depths
462 are less dependent on elevation, with snow depth values between 0 and 1 appearing at all elevations between 0 and 1250m. The
463 2DH analysis supports the findings from the snow depth distribution maps where the variability of snow depth observed in the RS
464 dataset is not replicated in the NoAssim case or the Best CSO simulation (Figure 7).
465



466
467
468
469
470

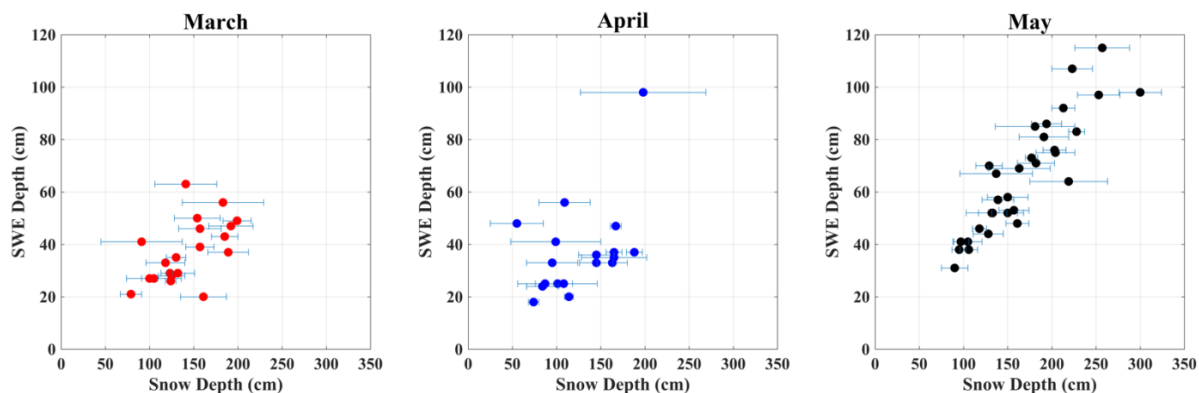
Figure 9: Two-dimensional Histograms.
The remote sensing (RS) dataset vs. the (a) water year (WY) 2017 no assimilation case, (b) WY2018 no assimilation case, (c) WY2017 best CSO simulation, and (d) WY2018 best CSO simulation.

471 6.3 Fieldwork 2018 Results

472 To validate the WY2018 SWE distributions from the NoAssim case and the Best CSO simulation we used ground-truth data from
473 our field campaign in April 2018. The locations of the 70 SWE and snow depth measurement sites from 2018 are depicted in
474 Figure 3. Figure 10 shows the co-located SWE depth measurements (y axes) versus the snow depth measurements (x axes) from
475 each site aggregated by month. The bars in Figure 10 represent the variability in snow depth within the surrounding 100m² of the
476 SWE measurement, including the average, minimum, and maximum of 8 snow depth measurements at each site. Table 3 shows
477 the results at the SWE measurement sites, comparing the NoAssim case versus the Best CSO simulation using RMSE, bias, and
478 mean absolute error (MAE) metrics for evaluation. Since each measurement site corresponds to a single CSO snow depth



479 submission, we separated those measurement sites used in the assimilation scheme from the validation set when creating Table 3.
 480 The Best CSO simulation outperforms the NoAssim case according to all metrics in all months. The 2018 fieldwork results from
 481 April show that the Best CSO simulation has a bias of +3 cm, while the NoAssim case is +97 cm. The April 2018 fieldwork results
 482 agree with the histogram and ECDF analysis that displayed broad overestimation of SWE in the NoAssim case in WY2018 (Figure
 483 7b; Figure 8d).
 484



485
 486
 487
 488
 489

Figure 10: Fieldwork 2018 Measurements by Month
 The 70 *in-situ* snow water equivalent (SWE) measurements (y axes) from 2018 are plotted by month along with their co-located snow depth measurements (x axes). The bars show the minimum, maximum, and average of each fieldwork site where 8 snow depth measurements were obtained in a 100 m² area.

490
 491
 492
 493

Table 3: Fieldwork 2018 Results
 The 70 SWE measurements from the 2018 fieldwork compared to the Best CSO simulation and the no assimilation (NoAssim) case using the three model performance metrics: root mean squared error (RMSE), mean bias error (Bias), and mean absolute error (MAE).

	Bias SWE (cm)		RMSE SWE (cm)		MAE SWE (cm)	
	Best CSO	NoAssim	Best CSO	NoAssim	Best CSO	NoAssim
All	-11	86	28	100	22	86
March	-3	77	15	95	13	77
April	3	97	21	114	16	97
May	-25	84	37	95	31	84

494

495 6.4 Spatially Averaged Snow Water Equivalent Results

496 Another way to quantify the ability of CSO measurements to constrain SnowModel output is to investigate the modeled SWE
 497 averaged over a large area. Table 4 contains the spatially averaged SWE estimations from the RS survey area in WY2018, and
 498 includes the RS dataset, the Best CSO simulation, and the NoAssim case. We focus on WY2018 because the fieldwork
 499 measurements include estimated bulk density values at each measurement site. These bulk density estimations were measured
 500 during April 2018 and were partitioned from the larger dataset and spatially averaged over the RS region only (n=22). The
 501 fieldwork estimated bulk density value was then applied to the spatially averaged RS snow depth. For the Best CSO simulation
 502 and the NoAssim case, the spatially averaged snow depth, SWE, and snow density values were taken directly from the model



503 results. The SWE estimation results in Table 4 demonstrate that SnowAssim can constrain the SWE output over a large region
504 based on a few, randomly chosen CSO measurements. Importantly, the accuracy of the total modeled water volume from the RS
505 region in 2018 improves when CSO measurements are included, a key finding that has implications for water resource management
506 decisions in snowy, data-limited, mountain environments.

507

508

509 **Table 4: Spatially Averaged Variables in the RS Region**
510 **The spatially averaged results were calculated using the RS region in WY2018, the RS dataset, and the modeled results. The spatially**
511 **averaged SWE depth for the RS survey was estimated using the average density measured during April 2018 fieldwork.**

Dataset	Spatially Averaged Snow Depth (cm)	Spatially Averaged Density (kg/m ³)	Spatially Averaged SWE Depth (cm)	Total RS Region Water Volume (km ³)
RS Survey 2018	130 (RS survey)	331 (fieldwork)	43 (estimated)	0.06 (estimated)
Best CSO Simulation 2018	130 (modeled)	400 (modeled)	52 (modeled)	0.08 (modeled)
NoAssim 2018	267 (modeled)	430 (modeled)	115 (modeled)	0.17 (modeled)

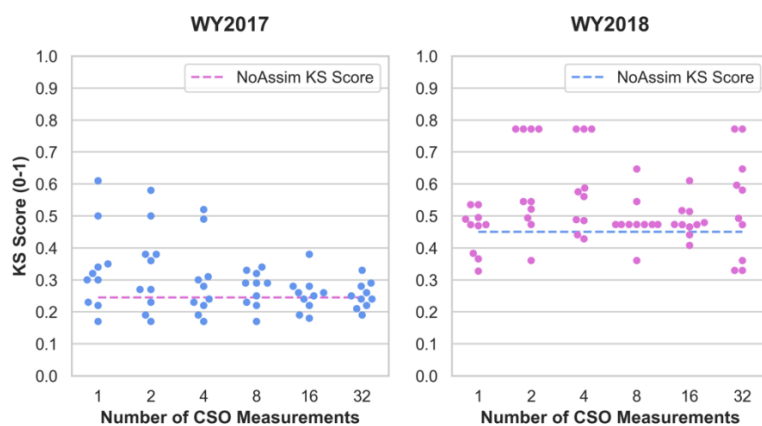
511

512

513 6.5 Precipitation Adjustment Experiment

514 The experimental design of the present study was developed for remote locations where a long-term precipitation dataset was not
515 available to bias correct the precipitation inputs. However, since a long-term precipitation dataset may be available in other
516 locations, we decided to test the results with a precipitation experiment. In this experiment we applied a scalar to the CFSv2
517 precipitation fields for bias correction and all other model parameters and input datasets were held constant. The experiment results
518 show that some of the CSO ensemble simulations still outperformed the NoAssim case with the precipitation adjustment, both
519 spatially and temporally. For example, the spatial results show that 43% percent of the ensemble runs in WY2017 and 20% of the
520 ensemble runs in WY2018 outperformed the NoAssim case when the precipitation was bias corrected, according to their KS score
521 (Figure 11). Similarly, the temporal results show that 42% of the ensemble runs in WY2017 and 58% of the ensemble runs in
522 WY2018 outperformed the NoAssim case when the precipitation was bias corrected, according to their KGE score. The ECDF
523 and histogram analysis from the precipitation adjustment factor experiment also show model improvements when there was broad
524 underestimation of snow depths in the NoAssim case in WY2017 and broad overestimation in WY2018. These results demonstrate
525 that using CSO measurements for assimilation can improve model performance when the available weather forcing dataset has
526 known biases (no precipitation adjustment factor case) but when those biases have been decreased (precipitation adjustment factor
527 case) the improvements become less clear, they vary from year to year, and are less consistent between spatial and temporal results.

528



529
530
531
532
533
534

Figure 11: Swarmplots of Kolmogorov-Smirnov Scores with Precipitation Adjustment Factor.
The ensemble simulations are ranked by Kolmogorov-Smirnov (KS) score per water year (WY) and plotted according to the number of CSO measurements assimilated, including the no assimilation (NoAssim) case.

535 7 Discussion

536 An important consideration in the results of the present study involves ranking the CSO ensemble members by various spatial and
537 temporal metrics. The time series results (Section 6.1), the spatially distributed results (Section 6.2), and the spatially averaged
538 results (Section 6.4) did not have the same ranking order for the CSO ensemble members. For example, the Best CSO simulation
539 in WY2017 from the time-series analysis was an ensemble member with two CSO measurements assimilated according to the
540 KGE metric. The time-series results represent a single point in the domain, the UTS station. By contrast, the Best CSO simulation
541 in WY2017 from the spatial distribution analysis was an ensemble member with eight CSO measurements assimilated using the
542 KS score. The spatially distributed results represent the entire RS survey area. The improvements in model performance are
543 determined by the type of validation dataset available and the metric used to quantify those improvements. In other words, one
544 size does not fit all when it comes to quantifying improvements to model performance using CSO measurements.

545

546 The variability of snow depth and SWE in mountain catchments and the spatial patterning of snowpack conditions in complex
547 terrain is a well-known challenge in snow modeling and snow remote sensing research (Anderton et al., 2004; Lopez-Moreno et
548 al., 2013; Luce et al., 1998; Molotch et al., 2005; Rice and Bales, 2010; Sturm et al., 2010b). The RS results reveal that variability
549 in snow depth across short distances is largely a function of wind redistribution and drifting and not primarily a function of elevation
550 (Figure 9c,f; Figure 7a,b). Thompson Pass is a notoriously windy location, and the RS dataset shows complex drifting patterns
551 throughout the surveyed area (Figure 7a,b). The wind inputs from the reanalysis product used in Micromet and SnowTran3d may
552 not be adequate for the steepness and ruggedness of the terrain. Although wind scaling factors were tested in the calibration, the
553 only suitable calibration dataset was the SNOTEL site. SNOTEL stations are often situated in locations where the effects of wind
554 redistribution of the snowpack are dampened and SNOTEL station data are often not representative of the spatial variability of the
555 surrounding areas (Dressler et al., 2006; Molotch and Bales, 2005). The inability of SnowTran3d to resolve the wind



556 redistribution of the snowpack more accurately, the course wind field inputs from the reanalysis products, and the use of a single
557 SNOTEL station for calibration, together represent a model and input data limitation of the current study.

558

559 The ensemble results highlight a deeper question in snow hydrology and process modeling in general, regarding the sub-grid scale
560 variability of the modeled state variable within a single model grid cell. The scale of the *in-situ* observations (measured with an
561 avalanche probe) and the scale of the model resolution (30 m grid) versus the scale of the physical process being modeled (true
562 patterns and true variance in space and time) can create scale effects that need to be accounted for (Blöschl et al., 1999). In this
563 way, the 2018 fieldwork has a significant role to play in our understanding of the sub-grid scale variability in snow depth
564 distributions. CSO participants average a few point measurements over a 1-4 m² area. The model resolution is 30 m, or 900 m² per
565 grid model grid cell. If participants move slightly one direction or another, their averaged and submitted measurements would
566 likely be different, but their measurements would potentially lie within the same 30 m model grid cell. This difference, in turn,
567 would modify the SWE depth inputs for SnowAssim. To better characterize the sub-grid scale variability of snow depth we
568 investigate the 8 avalanche probe depths taken over 100 m² at each of the 70 observation sites during the 2018 fieldwork (see also
569 Figure 11). From these data, a picture of the sub-grid scale variability emerges. The largest range in snow depth values at a single
570 100 m² observation site is 2.11 m and the smallest range in snow depth values at a single site is 0.09 m. The highest standard
571 deviation (sd) found at a single observation site is 0.71 m and the lowest sd is 0.04 m. This shows that a significant amount of
572 variation, and therefore uncertainty, is being added to the model chain simply by the sub-grid scale variability of snow depth
573 distributions within a single model grid cell, distributions that the model will not be able to resolve at the 30 m or 100 m resolution.
574 Sub-grid scale variability is a well known problem in snow science and represents a limitation of the improvements that can be
575 made by assimilating CSO measurements (Elder et al., 1993, Blöschl et al., 1999; Liston et al., 2008; Schmucki et al., 2013).

576

577 One of the limitations of the present study is that the physical and temporal characteristics of the CSO measurements like aspect,
578 elevation, and early-season measurements were not fully tested. Initial simulations demonstrated that SnowAssim performs best
579 when the assimilated measurements were located close in time to the validation dataset. This factor influenced our choice to focus
580 on the late-season time period of CSO measurements since the RS surveys were conducted in the late-season. Additionally, since
581 the majority of the CSO measurements for both WYs occurred between March 15th and May 15th, future research should be in a
582 location where CSO measurements are obtained frequently throughout the accumulation season. A research project with many
583 measurements throughout the accumulation period may provide more insights into the temporal aspects of assimilation of CSO
584 measurements. We decided not to subset the CSO measurements by geophysical characteristics like aspect, elevation, and land
585 cover type because these require additional analysis that is outside of the scope of the current study. Understanding the effects of
586 temporal and spatial restrictions of CSO measurements on model performance will likely be an area of future research.
587 Additionally, it may be necessary to test other process models and alternate assimilation schemes in the future to improve the
588 spatial distribution of model results and determine if CSO measurements can be used in other modeling contexts.

589

590 **7 Conclusions**

591 In this study we use a new snow dataset collected by participants in the Community Snow Observations (CSO) project in coastal
592 Alaska to improve snow depth and snow water equivalence (SWE) outputs from a snow process model. Ensemble simulations



593 were carried out during the 2017 and 2018 snow seasons to investigate the effects of incorporating citizen science measurements
 594 into the model chain using an assimilation scheme. Time series SNOTEL station records, remotely sensed photogrammetry and
 595 light detection and ranging surveys, and fieldwork observations are used to validate the modeled snow depth and snow water
 596 equivalent distributions. Any number of CSO measurements assimilated improves model performance, from 1 to 32. Our results
 597 demonstrate that using CSO measurements for assimilation can improve model performance when the available weather forcing
 598 dataset has known biases and also when those biases have been decreased by using a precipitation adjustment factor. The
 599 improvements in model performance from CSO measurements occur in 62% to 78% of the ensemble simulations both spatially
 600 and temporally, and in cases when the model broadly overestimates or underestimates snow depth and SWE. Model estimations
 601 of total water volume from a sub-region of the study area also demonstrate improvements in accuracy after CSO measurements
 602 have been assimilated. This study has implications for water resource management and snow modeling in locations where *in-situ*
 603 snow information is limited but snow enthusiasts often visit, since even small numbers of assimilated CSO measurements can
 604 improve the snow model outputs.

605 8 Appendices

606 **Appendix A: Model calibration parameters and their descriptions.**

Parameter	# of Options	Format	Description
Temperature Lapse Rate	3 sets	Monthly	PRISM Climatologies; Local Weather Station Data; SnowModel Default
Precipitation Lapse Rate	5 sets	Monthly	Monthly Coefficients of 1/4, 1/2, 3/4, 1(SnowModel Default), PRISM Climatologies
Wind Adjustment Factor	3	Coefficient	Coefficients of 1(SnowModel Default),2,3
SnowTran3d	2	On/Off	

607

608

609

Appendix B: Top performing parameter configurations from the calibration simulations.

Rank	Temperature Lapse Rate	Precipitation Scaling Factor	Wind Adjustment Factor	SnoTran on/off
Tied for first	Default	Default	Default	On
Tied for first	Local Weather Station	Default	Default	On
Tied for first	PRISM Climatologies	Default	Default	On

610

611

612

613

614

Appendix C: Precipitation Adjustment Factor Results.

The best precipitation adjustment factors are shown, along with the root mean squared error (RMSE), the Nash Sutcliffe Efficiency (NSE), the Kling-Gupta Efficiency (KGE), and the mean bias error (Bias).

Reanalysis, Resolution	Time Period (WY)	Time Step	Number of Simulations	Precipitation Adjustment Factor	RMSE Precipitation (mm)	NSE	KGE	Bias Precipitation (+/- mm)
MERRA2, 30m	2012-2016	3hrly	11	0.55	7.5	0.07	0.20	0.0
MERRA2, 100m	2012-2016	3hrly	11	0.55	7.5	0.07	0.20	0.0
CFSv2, 30m	2012-2016	6hrly	11	0.60	6.7	0.27	0.35	-0.1
CFSv2, 100m	2012-2016	6hrly	11	0.60	6.7	0.27	0.35	-0.1



615
 616
 617
 618
 619
 620

Appendix D: Ranked Temporal Results.
Ensemble results from ranked by Kling-Gupta efficiency (KGE) score for water year (WY) 2017 (a) and WY2018 (b). Also included are the Nash Sutcliffe Efficiency (NSE) and the mean bias error (Bias) values.

(a) WY2017

Rank	Number of CSO Measurements	Iteration	KGE	NSE	Bias (cm)
1	2	2	0.97	0.99	0
2	1	8	0.97	0.99	0
3	4	1	0.94	0.93	0
4	2	6	0.93	0.92	0
5	8	9	0.93	0.89	-1
6	16	8	0.90	0.84	-1
7	32	3	0.88	0.96	-1
8	4	4	0.88	0.91	-2
9	1	10	0.80	0.95	-3
10	4	3	0.80	0.89	2
11	16	2	0.78	0.82	-3
12	8	1	0.77	0.81	2
13	32	8	0.77	0.79	-3
14	2	8	0.77	0.93	-3
15	16	7	0.76	0.93	-3
16	16	1	0.75	0.87	-3
17	4	6	0.74	0.92	-3
18	1	6	0.71	0.89	4
19	16	3	0.67	0.88	-4
20	32	4	0.66	0.79	-5
21	32	5	0.65	0.78	-5
22	32	1	0.65	0.78	-5
23	32	7	0.64	0.80	-5
24	2	3	0.63	0.80	4
25	4	9	0.62	0.83	-5
26	16	9	0.62	0.82	-5
27	2	10	0.61	0.82	-5
28	16	4	0.60	0.75	-5
29	32	6	0.59	0.82	-5
30	8	8	0.59	0.76	5
31	32	2	0.57	0.78	6
32	16	5	0.56	0.73	-6
33	4	8	0.56	0.73	-6
34	8	10	0.55	0.72	-6
35	8	7	0.54	0.73	-6
36	16	6	0.54	0.70	-6
37	1	3	0.54	0.74	6
38	8	2	0.52	0.68	-6
39	8	4	0.52	0.71	-6
40	1	2	0.51	0.72	-6
41	4	10	0.50	0.67	-7
42	32	10	0.49	0.66	-7
43	4	7	0.46	0.63	-7
NoAssim	NoAssim	NoAssim	0.47	0.66	7
44	8	3	0.43	0.66	-7
45	32	9	0.41	0.63	-8
46	8	5	0.39	0.54	-8
47	2	1	0.36	0.53	-8
48	8	6	0.34	0.49	-9
49	1	4	0.33	0.49	-9
50	1	7	0.29	0.42	-9



51	2	4	0.28	0.41	-9
52	16	10	0.26	0.37	-10
53	2	5	0.22	0.32	-10
54	1	5	0.17	0.23	-11
55	1	9	0.08	0.05	-12
56	2	7	0.08	0.05	-12
57	4	2	0.06	0.02	-12
58	4	5	0.03	-0.03	-12
59	2	9	-0.02	-0.13	-13
60	1	1	-0.07	-0.24	-14

621

622

(b) WY2018

Rank	Number of CSO Measurements	Iteration	KGE	NSE	Bias (m)
1	2	7	0.95	0.96	0
2	8	9	0.91	0.90	2
3	8	5	0.90	0.89	2
4	2	9	0.88	0.91	2
5	2	4	0.87	0.93	-2
6	4	7	0.87	0.97	3
7	4	8	0.84	0.97	-2
8	1	5	0.84	0.95	-2
9	1	6	0.84	0.95	-2
10	4	10	0.82	0.95	4
11	2	2	0.77	0.92	5
12	4	9	0.77	0.88	-4
13	16	9	0.76	0.85	-4
14	16	5	0.76	0.53	-2
15	16	4	0.76	0.53	-2
16	4	6	0.75	0.84	-4
17	32	10	0.74	0.49	-2
18	4	5	0.71	0.72	-5
19	2	6	0.71	0.89	6
20	1	8	0.71	0.83	-5
21	1	1	0.71	0.83	-5
22	1	9	0.71	0.83	-5
23	8	7	0.69	0.80	-6
24	16	8	0.68	0.58	-6
25	16	2	0.65	0.77	-6
26	32	2	0.65	0.53	-6
27	32	5	0.64	0.50	-6
28	32	8	0.64	0.49	-6
29	32	7	0.62	0.47	-6
30	32	9	0.62	0.47	-6
31	32	4	0.62	0.46	-6
32	32	1	0.62	0.46	-6
33	8	10	0.57	0.42	-7
34	4	1	0.53	0.65	-9
35	2	1	0.52	0.65	-9
36	32	3	0.49	0.18	6
37	4	4	0.48	0.60	-10
38	4	2	0.47	0.60	-10
39	4	3	0.45	0.57	-10
40	8	6	0.43	0.52	11
41	2	3	0.38	0.46	-11
42	1	7	0.33	0.38	-12
43	8	4	0.30	0.29	-13
44	1	2	0.30	0.36	15
45	16	1	0.24	0.14	-14
46	32	6	0.24	0.13	-14
47	1	4	0.23	0.29	16



48	1	10	0.07	-0.09	-17
49	8	8	0.01	-0.21	-18
50	8	3	0.00	-0.24	-18
51	1	3	-0.07	-0.37	-20
52	16	3	-0.15	-1.18	18
53	16	7	-0.16	-1.15	18
54	16	6	-0.16	-1.15	18
55	8	1	-0.16	-1.14	18
56	16	10	-0.16	-1.13	19
57	2	8	-0.23	-1.05	21
58	8	2	-0.28	-1.07	23
59	2	5	-0.37	-1.18	27
60	2	10	-0.58	-2.00	32

623

624

625

626 **Appendix E: Ranked Spatial Results.**
 627 **Spatial distribution ensemble results ranked by Kolmogorov-Smirnov (KS) score for water year (WY) 2017 (a) and WY2018 (b). Also**
 628 **included are the root mean squared error (RMSE) and the median values.**

628

(a) WY2017 Results

Rank	Number of CSO Measurements	Iteration	KS Score (0 - 1)	RMSE (m)	Median (m)	Mean (m)
1	8	9	0.17	1.171	1.071	1.198
2	1	8	0.17	1.173	1.066	1.192
3	2	2	0.17	1.173	1.064	1.190
4	4	1	0.18	1.164	1.096	1.225
5	2	6	0.19	1.159	1.116	1.248
6	4	4	0.19	1.202	0.983	1.100
7	32	2	0.21	1.149	1.156	1.393
8	32	3	0.21	1.222	0.931	1.044
9	8	8	0.21	1.148	1.166	1.402
10	1	10	0.22	1.243	0.888	0.995
11	16	8	0.22	1.287	0.693	0.883
12	16	1	0.23	1.251	0.872	0.978
13	2	8	0.23	1.256	0.861	0.966
14	4	2	0.23	1.135	1.250	1.396
15	4	3	0.23	1.135	1.250	1.396
16	4	6	0.24	1.267	0.840	0.942
17	16	7	0.24	1.270	0.834	0.936
18	8	1	0.24	1.133	1.281	1.430
19	1	6	0.24	1.133	1.281	1.430
20	16	2	0.25	1.321	0.651	0.814
21	32	4	0.25	1.293	0.801	0.891
22	32	5	0.25	1.293	0.794	0.892
23	16	3	0.26	1.306	0.770	0.866
24	32	1	0.26	1.310	0.761	0.855
25	32	7	0.27	1.316	0.754	0.847
26	4	9	0.27	1.320	0.749	0.843
27	16	4	0.27	1.324	0.738	0.832
28	2	10	0.27	1.328	0.731	0.825
29	16	9	0.27	1.328	0.730	0.824
30	2	3	0.27	1.135	1.406	1.567
31	8	10	0.28	1.344	0.715	0.804
32	1	3	0.28	1.137	1.426	1.589
33	16	5	0.28	1.349	0.696	0.788
34	4	8	0.29	1.350	0.694	0.786
35	32	6	0.29	1.351	0.692	0.784
36	16	6	0.29	1.355	0.685	0.777
37	8	7	0.29	1.360	0.678	0.769
NoAssim	NoAssim	NoAssim	0.30	1.145	1.482	1.651
38	8	2	0.30	1.370	0.663	0.753



39	32	10	0.30	1.384	0.649	0.731
40	1	2	0.30	1.381	0.644	0.734
41	4	10	0.30	1.384	0.639	0.729
42	32	8	0.31	1.404	0.461	0.667
43	8	4	0.31	1.400	0.614	0.703
44	4	7	0.32	1.402	0.612	0.701
45	8	3	0.33	1.426	0.573	0.662
46	8	5	0.34	1.438	0.565	0.649
47	32	9	0.34	1.448	0.546	0.630
48	8	6	0.35	1.469	0.521	0.603
49	2	1	0.36	1.468	0.514	0.600
50	1	4	0.37	1.484	0.490	0.576
51	1	7	0.38	1.510	0.453	0.539
52	2	4	0.38	1.510	0.453	0.539
53	16	10	0.39	1.529	0.426	0.512
54	2	5	0.41	1.559	0.385	0.472
55	1	5	0.44	1.601	0.330	0.418
56	1	9	0.50	1.684	0.223	0.314
57	2	7	0.50	1.684	0.223	0.314
58	4	5	0.53	1.724	0.175	0.268
59	2	9	0.57	1.770	0.119	0.217
60	1	1	0.61	1.812	0.067	0.173

629

630

631

632

633

(b) WY2018 Results

Rank	Number of CSO Measurements	Iteration	KS Score (0 - 1)	RMSE (m)	Median (m)	Mean (m)
1	1	10	0.30	1.210	0.838	0.905
2	8	3	0.34	1.246	0.756	0.810
3	8	8	0.34	1.246	0.756	0.810
4	1	7	0.38	1.146	1.124	1.238
5	16	1	0.38	1.150	1.127	1.237
6	32	6	0.38	1.150	1.127	1.237
7	8	4	0.38	1.150	1.127	1.237
8	2	3	0.39	1.146	1.182	1.304
9	1	3	0.41	1.319	0.621	0.655
10	4	3	0.41	1.153	1.261	1.392
11	4	1	0.42	1.147	1.292	1.437
12	4	2	0.42	1.155	1.279	1.413
13	4	4	0.42	1.165	1.305	1.435
14	2	1	0.43	1.166	1.335	1.474
15	8	7	0.46	1.205	1.487	1.651
16	16	2	0.47	1.261	1.568	1.708
17	1	1	0.47	1.221	1.521	1.684
18	1	9	0.47	1.221	1.521	1.684
19	1	8	0.47	1.221	1.523	1.686
20	16	8	0.48	1.233	1.553	1.746
21	32	1	0.48	1.233	1.553	1.746
22	32	2	0.48	1.233	1.553	1.746
23	32	4	0.48	1.233	1.553	1.746
24	32	5	0.48	1.233	1.553	1.746
25	32	7	0.48	1.233	1.553	1.746
26	32	8	0.48	1.233	1.553	1.746
27	32	9	0.48	1.233	1.553	1.746
28	4	9	0.48	1.244	1.577	1.753
29	4	5	0.48	1.248	1.580	1.748
30	4	6	0.48	1.248	1.580	1.748
31	1	5	0.49	1.259	1.607	1.780



32	1	6	0.49	1.259	1.607	1.780
33	4	8	0.49	1.259	1.607	1.780
34	8	10	0.49	1.259	1.607	1.780
35	16	9	0.49	1.281	1.628	1.801
36	2	4	0.51	1.318	1.714	1.893
37	2	7	0.53	1.353	1.777	1.968
38	16	4	0.54	1.401	1.848	2.068
39	16	5	0.54	1.401	1.848	2.068
40	32	10	0.54	1.401	1.848	2.068
41	8	9	0.55	1.453	1.922	2.131
42	4	7	0.55	1.454	1.928	2.132
43	2	9	0.56	1.461	1.939	2.148
44	8	5	0.56	1.500	1.977	2.189
45	4	10	0.56	1.493	1.980	2.191
46	2	2	0.58	1.540	2.043	2.263
47	2	6	0.59	1.606	2.128	2.350
NoAssim	NoAssim	NoAssim	0.64	1.861	2.411	2.678
48	1	2	0.65	1.894	2.436	2.721
49	32	3	0.65	1.928	2.466	2.764
50	8	6	0.65	1.928	2.466	2.764
51	1	4	0.66	2.009	2.567	2.852
52	16	10	0.77	2.932	3.466	3.839
53	16	3	0.77	2.932	3.466	3.839
54	16	6	0.77	2.932	3.466	3.839
55	16	7	0.77	2.932	3.466	3.839
56	2	10	0.77	2.932	3.466	3.839
57	2	5	0.77	2.932	3.466	3.839
58	2	8	0.77	2.932	3.466	3.839
59	8	1	0.77	2.932	3.466	3.839
60	8	2	0.77	2.932	3.466	3.839

634

635 9 Code and Data Availability

636 The datasets used in this study can be found at the following locations.

637

638 1. Community Snow Observations website and snow depth data download at <http://app.communitysnowobs.org/>
 639 (last accessed 30 April 2020).

640

641 2. The snow depth to snow water equivalence calculator (Hill et al., 2019) can be downloaded via Github at
 642 <https://github.com/communitysnowobs/snowdensity> (last accessed: 30 April 2020).

643

644 3. Snow Telemetry data for the Upper Tsaina River station near Valdez, Alaska is available at the Natural Resources
 645 Conservation Service website: <https://wcc.sc.egov.usda.gov/nwcc/site?sitenum=1055> (last accessed: 30 April 2020).

646

647 4. Climate Forecast System Reanalysis version 2 (CFSv2) data (Saha et al., 2011) is available for download at
 648 <https://rda.ucar.edu/datasets/ds094.0/#!description>.

649

650 5. The CFSv2 data was accessed using Google Earth Engine at [https://developers.google.com/earth-](https://developers.google.com/earth-engine/datasets/catalog/NOAA_CFSV2_FOR6H)
 651 [engine/datasets/catalog/NOAA_CFSV2_FOR6H](https://developers.google.com/earth-engine/datasets/catalog/NOAA_CFSV2_FOR6H) (last accessed: 30 April 2020). A javascript version of the Earth Engine



652 code written for this project is available at https://github.com/snowmodel-tools/preprocess_javascript (last accessed: 30
653 April 2020).

654

655 6. To convert the CFSv2 data downloaded from Google Earth Engine to the necessary input file for MicroMet we
656 wrote Matlab scripts that can be downloaded via Github at https://github.com/snowmodel-tools/preprocess_matlab (last
657 accessed: 30 April 2020).

658

659 7. The MERRA2 weather reanalysis product from NASA's Global Modeling and Assimilation office (Gelaro et
660 al., 2017) can be downloaded at https://gmao.gsfc.nasa.gov/reanalysis/MERRA-2/data_access/ (last accessed: 30 April
661 2020).

662

663 8. The National Elevation Dataset is (Gesch et al., 2002) available for download at
664 <https://catalog.data.gov/dataset/usgs-national-elevation-dataset-ned> (last accessed: 30 April 2020).

665

666 9. The National Land Cover Database 2011 dataset (Homer et al., 2011) is available for download at the Multi-
667 Resolution Land Characteristics Consortium at <https://www.mrlc.gov/data?f%5B0%5D=category%3Aland%20cover>
668 (last accessed: 30 April 2020).

669 **10 Author Contributions**

670 Ryan Crumley, David Hill, Gabriel Wolken, Katreen Wikstrom Jones, and Anthony Arendt designed the research questions and
671 decided on the methods. Ryan Crumley, Gabriel Wolken, Katreen Wikstrom Jones, and David Hill conducted fieldwork in the
672 study area, including snowpack sampling and remote sensing surveys. Ryan Crumley and Dave Hill oversaw the analysis of the
673 manuscript. Anthony Arendt designed and maintained the CSO website and snow dataset with contributions from all authors.
674 Community Snow Observation Participants and all authors contributed snow depth measurements. Ryan Crumley prepared the
675 manuscript with contributions from all authors during editing and review process.

676 **11 Competing Interests**

677 The authors declare that they have no conflicts of interest.

678 **12 Acknowledgements**

679 This research has been supported by NASA (grant no. NNX17AG67A) and CUAHSI (Pathfinder Fellowship grant). Arendt was
680 partially supported by the Washington Research Foundation, and by a Data Science Environments project award to the University
681 of Washington eScience Institute from the Gordon and Betty Moore and the Alfred P. Sloan Foundations.

682

683 **References**

684 Anderton, S.P., White, S.M. and Alvera, B.: Evaluation of spatial variability in snow water equivalent for a high mountain
685 catchment. *Hydrological Processes*, 18(3), pp.435-453, <https://doi.org/10.1002/hyp.1319>, 2004.

686



- 687 Bales, R.C., Molotch, N.P., Painter, T.H., Dettinger, M.D., Rice, R. and Dozier, J.: Mountain hydrology of the western United
688 States. *Water Resources Research*, 42(8), <https://doi.org/10.1029/2005WR004387>, 2006.
- 689
- 690 Baba, M., Gascoïn, S., Jarlan, L., Simonneaux, V. and Hanich, L.: Variations of the Snow Water Equivalent in the Ourika
691 Catchment (Morocco) over 2000–2018 Using Downscaled MERRA-2 Data. *Water*, 10(9), p.1120,
692 <https://doi.org/10.3390/w10091120>, 2018.
- 693
- 694 Barnes, S.L.: A technique for maximizing details in numerical weather map analysis, *Journal of Applied Meteorology*, 3(4),
695 pp.396-409, [https://doi.org/10.1175/1520-0450\(1964\)003<0396:ATFMDI>2.0.CO;2](https://doi.org/10.1175/1520-0450(1964)003<0396:ATFMDI>2.0.CO;2), 1964.
- 696
- 697 Barnes, S.L.: Mesoscale objective map analysis using weighted time-series observations, Technical Report, National Severe
698 Storms Lab., Norman, Oklahoma, 1973.
- 699
- 700 Barnett, T.P., Adam, J.C. and Lettenmaier, D.P.: Potential impacts of a warming climate on water availability in snow-dominated
701 regions. *Nature*, 438(7066), p.303, <https://doi.org/10.1038/nature04141>, 2005.
- 702
- 703 Beamer, J.P., Hill, D.F., Arendt, A. and Liston, G.E.: High-resolution modeling of coastal freshwater discharge and glacier mass
704 balance in the Gulf of Alaska watershed, *Water Resources Research*, 52(5), pp.3888-3909,
705 <https://doi.org/10.1002/2015WR018457>, 2016.
- 706
- 707 Beamer, J.P., Hill, D.F., McGrath, D., Arendt, A. and Kienholz, C.: Hydrologic impacts of changes in climate and glacier extent
708 in the Gulf of Alaska watershed, *Water Resources Research*, 53, pp.7502-7520, <https://doi.org/10.1002/2016WR020033>, 2017.
- 709
- 710 Blöschl, G., Kirnbauer, R.: An analysis of snow cover patterns in a small alpine catchment, *Hydrological Processes*, 6(1), pp.99-
711 109, <https://doi.org/10.1002/hyp.3360060109>, 1992.
- 712
- 713 Blöschl, G.: Scaling issues in snow hydrology. *Hydrological processes*, 13(14-15), pp.2149-2175,
714 [https://doi.org/10.1002/\(SICI\)1099-1085\(199910\)13:14/15<2149::AID-HYP847>3.0.CO;2-8](https://doi.org/10.1002/(SICI)1099-1085(199910)13:14/15<2149::AID-HYP847>3.0.CO;2-8), 1999.
- 715
- 716 Bohr, G.S. and Aguado, E.: Use of April 1 SWE measurements as estimates of peak seasonal snowpack and total cold-season
717 precipitation. *Water Resources Research*, 37(1), pp.51-60, <https://doi.org/10.1029/2000WR900256>, 2001.
- 718
- 719 Bonney, R., Cooper, C.B., Dickinson, J., Kelling, S., Phillips, T., Rosenberg, K.V. and Shirk, J.: Citizen science: a developing tool
720 for expanding science knowledge and scientific literacy. *BioScience*, 59(11), pp.977-984, <https://doi.org/10.1525/bio.2009.59.11.9>,
721 2009.
- 722
- 723 Bromwich, D.H., Wilson, A.B., Bai, L.S., Moore, G.W. and Bauer, P.: A comparison of the regional Arctic System Reanalysis
724 and the global ERA-Interim Reanalysis for the Arctic. *Quarterly Journal of the Royal Meteorological Society*, 142(695), pp.644-
725 658, <https://doi.org/10.1002/qj.2527>, 2016.
- 726
- 727 Bühler, Y., Adams, M.S., Bösch, R. and Stoffel, A.: Mapping snow depth in alpine terrain with unmanned aerial systems (UASs):
728 potential and limitations. *The Cryosphere*, 10(3), pp.1075-1088, <https://doi.org/10.5194/tc-10-1075-2016>, 2016.



- 729
- 730 Buytaert, W., Zulkafli, Z., Grainger, S., Acosta, L., Alemie, T.C., Bastiaensen, J., De Bièvre, B., Bhusal, J., Clark, J., Dewulf, A.
731 and Foggin, M.: Citizen science in hydrology and water resources: opportunities for knowledge generation, ecosystem service
732 management, and sustainable development. *Frontiers in Earth Science*, 2, p.26, <https://doi.org/10.3389/feart.2014.00026>, 2014.
- 733
- 734 Carroll, T., Cline, D., Fall, G., Nilsson, A., Li, L. and Rost, A.: NOHRSC operations and the simulation of snow cover properties
735 for the coterminous US. In *Proc. 69th Annual Meeting of the Western Snow Conf* (pp. 1-14), 2001.
- 736
- 737 Carrassi, A., Bocquet, M., Bertino, L. and Evensen, G.: Data assimilation in the geosciences: An overview of methods, issues, and
738 perspectives. *Wiley Interdisciplinary Reviews: Climate Change*, 9(5), p.e535, <https://doi.org/10.1002/wcc.535>, 2018.
- 739
- 740 Carter, S., Carter, P. and Levison, J.: Skier triggered surface hoar: A discussion of avalanche involvements during the 2006 Valdez
741 Chugach helicopter ski season. In *Proceedings of International Snow Science Workshop* (pp. 860-867), 2006.
- 742
- 743 Clark, M.P., Slater, A.G., Barrett, A.P., Hay, L.E., McCabe, G.J., Rajagopalan, B. and Leavesley, G.H.: Assimilation of snow
744 covered area information into hydrologic and land-surface models. *Advances in water resources*, 29(8), pp.1209-1221,
745 <https://doi.org/10.1016/j.advwatres.2005.10.001>, 2006.
- 746
- 747 Clark, M.P., Hendrikx, J., Slater, A.G., Kavetski, D., Anderson, B., Cullen, N.J., Kerr, T., Örn Hreinsson, E. and Woods, R.A.:
748 Representing spatial variability of snow water equivalent in hydrologic and land-surface models: A review. *Water Resources*
749 *Research*, 47(7), <https://doi.org/10.1029/2011WR010745>, 2011.
- 750
- 751 Contosta, A.R., Adolph, A., Burchsted, D., Burakowski, E., Green, M., Guerra, D., Albert, M., Dibb, J., Martin, M., McDowell,
752 W.H. and Routhier, M.: A longer vernal window: the role of winter coldness and snowpack in driving spring transitions and lags.
753 *Global change biology*, 23(4), pp.1610-1625, <https://doi.org/10.1111/gcb.13517>, 2017.
- 754
- 755 Cooper, C. B., Dickinson J., Phillips, T., and Bonney, R.: Citizen science as a tool for conservation in residential ecosystems.
756 *Ecology and Society* 12(2): 11. URL: <http://www.ecologyandsociety.org/vol12/iss2/art11/> (accessed 05 May 2020), 2007.
- 757
- 758 Crumley, R.L., Hill, D.F., Beamer, J.P. and Holzenthal, E.R.: Seasonal components of freshwater runoff in Glacier Bay, Alaska:
759 diverse spatial patterns and temporal change. *The Cryosphere*, 13(6), pp.1597-1619, <https://doi.org/10.5194/tc-13-1597-2019>,
760 2019.
- 761
- 762 Dickinson, J.L., Zuckerberg, B. and Bonter, D.N.: Citizen science as an ecological research tool: challenges and benefits. *Annual*
763 *review of ecology, evolution, and systematics*, 41, pp.149-172, <https://doi.org/10.1146/annurev-ecolsys-102209-144636>, 2010.
- 764
- 765 Dressler, K.A., Fassnacht, S.R. and Bales, R.C.: A comparison of snow telemetry and snow course measurements in the Colorado
766 River basin. *Journal of hydrometeorology*, 7(4), pp.705-712, <https://doi.org/10.1175/JHM506.1>, 2006.
- 767
- 768 Elder, K., Rosenthal, W. and Davis, R.E.: Estimating the spatial distribution of snow water equivalence in a montane watershed.
769 *Hydrological Processes*, 12(10-11), pp.1793-1808, [https://doi.org/10.1002/\(SICI\)1099-1085\(199808/09\)12:10/11<1793::AID-
770 HYP695>3.0.CO;2-K](https://doi.org/10.1002/(SICI)1099-1085(199808/09)12:10/11<1793::AID-HYP695>3.0.CO;2-K), 1998.



771
772 Fayad, A., Gascoïn, S., Faour, G., López-Moreno, J.I., Drapeau, L., Le Page, M. and Escadafal, R.: Snow hydrology in
773 Mediterranean mountain regions: A review. *Journal of Hydrology*, 551, pp.374-396, <https://doi.org/10.1016/j.jhydrol.2017.05.063>,
774 2017.
775
776 Fielen, M.N. and Lowry, C.S.: Social. Water—A crowdsourcing tool for environmental data acquisition. *Computers &*
777 *Geosciences*, 49, pp.164-169, <https://doi.org/10.1016/j.cageo.2012.06.015>, 2012.
778
779 Garnett, R. and Stewart, R.: Comparison of GPS units and mobile Apple GPS capabilities in an urban landscape. *Cartography and*
780 *Geographic Information Science*, 42(1), pp.1-8, <https://doi.org/10.1080/15230406.2014.974074>, 2015.
781
782 Gesch, D., Evans, G., Mauck, J., Hutchinson, J., Carswell Jr., W.J.: The National Map—Elevation: U.S. Geological Survey Fact
783 Sheet 2009-3053, 2009.
784
785 Gelaro, R., McCarty, W., Suárez, M.J., Todling, R., Molod, A., Takacs, L., Randles, C.A., Darmenov, A., Bosilovich, M.G.,
786 Reichle, R. and Wargan, K.: The modern-era retrospective analysis for research and applications, version 2 (MERRA-2). *Journal*
787 *of Climate*, 30(14), pp.5419-5454, <https://doi.org/10.1175/JCLI-D-16-0758.1>, 2017.
788
789 Haberkorn, A.: European Snow Booklet – an Inventory of Snow Measurements in Europe. *EnviDat*.
790 <https://doi.org/10.16904/envidat.59>, 2019.
791
792 Hall D.K., Riggs G.A., Salomonson V.V.: MODIS/Terra Snow Cover Daily L3 Global 500m Grid, Version 6. Boulder, CO: NASA
793 National Snow and Ice Data Center Distributed Active Archive Center, 2016.
794
795 Helmert, J., Lange, M., Dong, J., De Rosnay, P., Gustafsson, D., Churulin, E., Kurzeneva, E., Müller, R., Trentmann, J., Souverijns,
796 N. and Koch, R.: 1st Snow Data Assimilation Workshop in the framework of COST HarmoSnow ESSEM 1404. *Meteorologische*
797 *Zeitschrift*, 27(4), pp.325-333, <https://doi.org/10.1127/metz/2018/0906>, 2018.
798
799 Hendrixx, J., Johnson, J. and Shelly, C.: Using GPS tracking to explore terrain preferences of heli-ski guides. *Journal of outdoor*
800 *recreation and tourism*, 13, pp.34-43, <https://doi.org/10.1016/j.jort.2015.11.004>, 2016.
801
802 Han, E., Merwade, V. and Heathman, G.C.: Implementation of surface soil moisture data assimilation with watershed scale
803 distributed hydrological model. *Journal of hydrology*, 416, pp.98-117, <https://doi.org/10.1016/j.jhydrol.2011.11.039>, 2012.
804
805 Hill, D., Wolken, G., Wikstrom Jones K., Crumley, R., and Arendt, A.: Crowdsourcing snow depth data with citizen scientists,
806 *Eos*, 99, <https://doi.org/10.1029/2018EO108991>, 2018.
807
808 Hill, D.F., Burakowski, E.A., Crumley, R.L., Keon, J., Hu, J.M., Arendt, A.A., Wikstrom Jones, K. and Wolken, G.J.: Converting
809 snow depth to snow water equivalent using climatological variables. *The Cryosphere*, 13(7), pp.1767-1784, <https://doi.org/10.5194/tc-13-1767-2019>, 2019.
810
811



- 812 Holko, L., Gorbachova, L. and Kostka, Z.: Snow hydrology in central Europe. *Geography Compass*, 5(4), pp.200-218,
813 <https://doi.org/10.1111/j.1749-8198.2011.00412.x>, 2011.
- 814
- 815 Homer, C., Dewitz, J., Yang, L., Jin, S., Danielson, P., Xian, G., Coulston, J., Herold, N., Wickham, J. and Megown, K.:
816 Completion of the 2011 National Land Cover Database for the conterminous United States—representing a decade of land cover
817 change information. *Photogrammetric Engineering & Remote Sensing*, 81(5), pp.345-354, <https://doi.org/10.1016/S0099->
818 [1112\(15\)30100-2](https://doi.org/10.1016/S0099-1112(15)30100-2), 2015.
- 819
- 820 Jonas, T., Marty, C. and Magnusson, J.: Estimating the snow water equivalent from snow depth measurements in the Swiss Alps.
821 *Journal of Hydrology*, 378(1-2), pp.161-167, <https://doi.org/10.1016/j.jhydrol.2009.09.021>, 2009.
- 822
- 823 Johnson, J.B.: A theory of pressure sensor performance in snow. *Hydrological Processes*, 18(1), pp.53-64,
824 <https://doi.org/10.1002/hyp.1310>, 2003.
- 825
- 826 Johnson, J.B. and Schaefer, G.L.: The influence of thermal, hydrologic, and snow deformation mechanisms on snow water
827 equivalent pressure sensor accuracy. *Hydrological Processes*, 16(18), pp.3529-3542, <https://doi.org/10.1002/hyp.1236>, 2002.
- 828
- 829 Kalnay, E., Kanamitsu, M., Kistler, R., Collins, W., Deaven, D., Gandin, L., Iredell, M., Saha, S., White, G., Woollen, J. and Zhu,
830 Y.: The NCEP/NCAR 40-year reanalysis project, *Bulletin of the American meteorological Society*, 77(3), pp.437-471,
831 [https://doi.org/10.1175/1520-0477\(1996\)077<0437:TNYRP>2.0.CO;2](https://doi.org/10.1175/1520-0477(1996)077<0437:TNYRP>2.0.CO;2), 1996.
- 832
- 833 Kalnay, E.: Atmospheric modeling, data assimilation and predictability. Cambridge university press, 2003.
- 834
- 835 Kapnick, S. and Hall, A.: Causes of recent changes in western North American snowpack. *Climate Dynamics*, 38(9-10), pp.1885-
836 1899, <https://doi.org/10.1007/s00382-011-1089-y>, 2012.
- 837
- 838 King, J.M., Cabrera, A.R. and Kelly, R.E.: The Snowtweets Project: Communicating snow depth measurements from specialists
839 and non-specialists via mobile communication technologies and social networks. AGU Fall Meeting Abstracts, Bibcode:
840 2009AGUFMED11A0562K, 2009.
- 841
- 842 Lader, R., Bhatt, U.S., Walsh, J.E., Rupp, T.S. and Bieniek, P.A.: Two-meter temperature and precipitation from atmospheric
843 reanalysis evaluated for Alaska, *Journal of Applied Meteorology and Climatology*, 55(4), pp.901-922,
844 <https://doi.org/10.1175/JAMC-D-15-0162.1>, 2016.
- 845
- 846 Lehning, M., Bartelt, P., Brown, B., Russi, T., Stöckli, U. and Zimmerli, M. SNOWPACK model calculations for avalanche
847 warning based upon a new network of weather and snow stations. *Cold Regions Science and Technology*, 30(1-3), pp.145-157,
848 [https://doi.org/10.1016/S0165-232X\(99\)00022-1](https://doi.org/10.1016/S0165-232X(99)00022-1), 1999.
- 849
- 850 Lehning, M., Völksch, I., Gustafsson, D., Nguyen, T.A., Stähli, M. and Zappa, MALPINE3D: a detailed model of mountain surface
851 processes and its application to snow hydrology. *Hydrological Processes: An International Journal*, 20(10), pp.2111-2128,
852 <https://doi.org/10.1002/hyp.6204>, 2006.
- 853



- 854 Li, D., Wigmore, O., Durand, M.T., Vander-Jagt, B., Margulis, S.A., Molotch, N.P. and Bales, R.C.: Potential of Balloon
855 Photogrammetry for Spatially Continuous Snow Depth Measurements. *IEEE Geoscience and Remote Sensing Letters*,
856 <https://doi.org/10.1109/LGRS.2019.2953481>, 2019.
857
- 858 Liston, G.E. and Elder, K.: A distributed snow-evolution modeling system (SnowModel), *Journal of Hydrometeorology*, 7(6),
859 pp.1259-1276, <https://doi.org/10.1175/JHM548.1>, 2006a.
860
- 861 Liston, G.E. and Elder, K.: A meteorological distribution system for high-resolution terrestrial modeling (MicroMet), *Journal of*
862 *Hydrometeorology*, 7(2), pp.217-234, <https://doi.org/10.1175/JHM486.1>, 2006b.
863
- 864 Liston, G.E., Haehnel, R.B., Sturm, M., Hiemstra, C.A., Berezovskaya, S. and Tabler, R.D.: Simulating complex snow distributions
865 in windy environments using SnowTran-3D. *Journal of Glaciology*, 53(181), pp.241-256,
866 <https://doi.org/10.3189/172756507782202865>, 2007.
867
- 868 Liston, G.E. and Hiemstra, C.A.: A simple data assimilation system for complex snow distributions (SnowAssim). *Journal of*
869 *Hydrometeorology*, 9(5), pp.989-1004, <https://doi.org/10.1175/2008JHM871.1>, 2008.
870
- 871 Liston, G.E. and Hiemstra, C.A.: The changing cryosphere: Pan-Arctic snow trends (1979–2009). *Journal of Climate*, 24(21),
872 pp.5691-5712, <https://doi.org/10.1175/JCLI-D-11-00081.1>, 2011.
873
- 874 López-Moreno, J.I., Fassnacht, S.R., Heath, J.T., Musselman, K.N., Revuelto, J., Latron, J., Morán-Tejeda, E. and Jonas, T.: Small
875 scale spatial variability of snow density and depth over complex alpine terrain: Implications for estimating snow water equivalent.
876 *Advances in water resources*, 55, pp.40-52, <https://doi.org/10.1016/j.advwatres.2012.08.010>, 2013.
877
- 878 Lowry, C.S. and Fienen, M.N.: CrowdHydrology: crowdsourcing hydrologic data and engaging citizen scientists. *GroundWater*,
879 51(1), pp.151-156, <https://doi.org/10.1111/j.1745-6584.2012.00956.x>, 2013.
880
- 881 Luce, C.H., Tarboton, D.G. and Cooley, K.R.: The influence of the spatial distribution of snow on basin-averaged snowmelt.
882 *Hydrological Processes*, 12(10-11), pp.1671-1683, [https://doi.org/10.1002/\(SICI\)1099-1085\(199808/09\)12:10/11<1671::AID-
883 HYP688>3.0.CO;2-N](https://doi.org/10.1002/(SICI)1099-1085(199808/09)12:10/11<1671::AID-HYP688>3.0.CO;2-N), 1998.
884
- 885 Luojus, K., Pulliainen, J., Takala, M., Derksen, C., Rott, H., Nagler, T., Solberg, R., Wiesmann, A., Metsamaki, S., Malnes, E. and
886 Bojkov, B.: Investigating the feasibility of the GlobSnow snow water equivalent data for climate research purposes. In 2010 IEEE
887 International Geoscience and Remote Sensing Symposium (pp. 4851-4853), IEEE,
888 <https://doi.org/10.1109/IGARSS.2010.5741987>, 2010.
889
- 890 Magnusson, J., Gustafsson, D., Hüsler, F. and Jonas, T.: Assimilation of point SWE data into a distributed snow cover model
891 comparing two contrasting methods. *Water resources research*, 50(10), pp.7816-7835, <https://doi.org/10.1002/2014WR015302>,
892 2014.
893
- 894 Malik, M.J., van der Velde, R., Vekerdy, Z. and Su, Z. Assimilation of satellite-observed snow albedo in a land surface model.
895 *Journal of hydrometeorology*, 13(3), pp.1119-1130, <https://doi.org/10.1175/JHM-D-11-0125.1>, 2012.



896
897 Mankin, J.S., Viviroli, D., Singh, D., Hoekstra, A.Y. and Diffenbaugh, N.S.: The potential for snow to supply human water demand
898 in the present and future. *Environmental Research Letters*, 10(11), p.114016, <https://doi.org/>, 2015.
899
900 Marks, D., Domingo, J., Susong, D., Link, T. and Garen, D.: A spatially distributed energy balance snowmelt model for application
901 in mountain basins, *Hydrological Processes*, 13(12-13), pp.1935-1959, [https://doi.org/10.1002/\(SICI\)1099-](https://doi.org/10.1002/(SICI)1099-)
902 1085(199909)13:12/13<1935::AID-HYP868>3.0.CO;2-C, 1999.
903
904 Massey Jr, F.J.:The Kolmogorov-Smirnov test for goodness of fit. *Journal of the American statistical Association*, 46(253), pp.68-
905 78, 1951.
906
907 McCreight, J.L., Small, E.E. and Larson, K.M.: Snow depth, density, and SWE estimates derived from GPS reflection data:
908 Validation in the western US. *Water Resources Research*, 50(8), pp.6892-6909, <https://doi.org/10.1002/2014WR015561>, 2014.
909
910 McLaughlin, D.: An integrated approach to hydrologic data assimilation: interpolation, smoothing, and filtering. *Advances in*
911 *Water Resources*, 25(8), pp.1275-1286, [https://doi.org/10.1016/S0309-1708\(02\)00055-6](https://doi.org/10.1016/S0309-1708(02)00055-6), 2002.
912
913 McKinley, D.C., Miller-Rushing, A.J., Ballard, H.L., Bonney, R., Brown, H., Cook-Patton, S.C., Evans, D.M., French, R.A.,
914 Parrish, J.K., Phillips, T.B. and Ryan, S.F.: Citizen science can improve conservation science, natural resource management, and
915 environmental protection. *Biological Conservation*, 208, pp.15-28, <https://doi.org/10.1016/j.biocon.2016.05.015>, 2017.
916
917 McMillan, H.K., Hreinsson, E.Ö., Clark, M.P., Singh, S.K., Zammit, C. and Uddstrom, M.J.: Operational hydrological data
918 assimilation with the recursive ensemble Kalman filter. *Hydrology and Earth System Sciences*, 17(1), pp.21-38,
919 <https://doi.org/10.5194/hess-17-21-2013>, 2013.
920
921 Mernild, S.H., Liston, G.E., Hasholt, B. and Knudsen, N.T.: Snow distribution and melt modeling for Mittivakkat Glacier,
922 Ammassalik Island, southeast Greenland. *Journal of Hydrometeorology*, 7(4), pp.808-824, <https://doi.org/10.1175/JHM522.1>,
923 2006.
924
925 Mernild, S.H., Liston, G.E., Hiemstra, C.A., Malmros, J.K., Yde, J.C. and McPhee, J.: The Andes Cordillera. Part I: snow
926 distribution, properties, and trends (1979–2014), *International Journal of Climatology*, 37(4), pp.1680-1698,
927 <https://doi.org/10.1002/joc.4804>, 2017a.
928
929 Mernild, S.H., Liston, G.E., Hiemstra, C.A., Yde, J.C., McPhee, J. and Malmros, J.K.: The Andes Cordillera. Part II: Rio Olivares
930 Basin snow conditions (1979–2014), central Chile, *International Journal of Climatology*, 37(4), pp.1699-1715,
931 <https://doi.org/10.1002/joc.4828>, 2017b.
932
933 Mesinger, F., DiMego, G., Kalnay, E., Mitchell, K., Shafran, P.C., Ebisuzaki, W., Jović, D., Woollen, J., Rogers, E., Berbery, E.H.
934 and Ek, M.B.: North American regional reanalysis, *Bulletin of the American Meteorological Society*, 87(3), pp.343-360,
935 <https://doi.org/10.1175/BAMS-87-3-343>, 2006.
936



- 937 Molotch, N.P. and Bales, R.C.: Scaling snow observations from the point to the grid element: Implications for observation network
938 design. *Water Resources Research*, 41(11), <https://doi.org/10.1029/2005WR004229>, 2005.
- 939
- 940 Molotch, N.P., Colee, M.T., Bales, R.C. and Dozier, J.: Estimating the spatial distribution of snow water equivalent in an alpine
941 basin using binary regression tree models: the impact of digital elevation data and independent variable selection. *Hydrological
942 Processes: An International Journal*, 19(7), pp.1459-1479, <https://doi.org/10.1002/hyp.5586>, 2005.
- 943
- 944 Mote, P.W., Li, S., Lettenmaier, D.P., Xiao, M. and Engel, R.: Dramatic declines in snowpack in the western US. *Npj Climate and
945 Atmospheric Science*, 1(1), pp.1-6, <https://doi.org/10.1038/s41612-018-0012-1>, 2018.
- 946
- 947 NOHRSC: Snow Data Assimilation System (SNODAS) Data Products at NSIDC, Version 1. Boulder, Colorado USA. NSIDC:
948 National Snow and Ice Data Center. doi: <https://doi.org/10.7265/N5TB14TC>, 2004.
- 949
- 950 Pagano, T., Garen, D., Perkins, T., and Pasteris, P.: Daily updating of operational statistical seasonal water supply forecasts for the
951 western U.S., *J. Am. Water Resour. As.*, 45, 767–778, <https://doi.org/10.1111/j.1752-1688.2009.00321.x>, 2009.
- 952
- 953 Painter, T.H., Berisford, D.F., Boardman, J.W., Bormann, K.J., Deems, J.S., Gehrke, F., Hedrick, A., Joyce, M., Laidlaw, R.,
954 Marks, D. and Mattmann, C.: The Airborne Snow Observatory: Fusion of scanning lidar, imaging spectrometer, and physically-
955 based modeling for mapping snow water equivalent and snow albedo. *Remote Sensing of Environment*, 184, pp.139-152,
956 <https://doi.org/10.1016/j.rse.2016.06.018>, 2016.
- 957
- 958 Park, S.K. and Xu, L. eds.: Data assimilation for atmospheric, oceanic and hydrologic applications (Vol. 2). Springer Science &
959 Business Media, 2013.
- 960
- 961 Pistocchi, A.: Simple estimation of snow density in an Alpine region. *Journal of Hydrology: Regional Studies*, 6, pp.82-89,
962 <https://doi.org/10.1016/j.ejrh.2016.03.004>, 2016.
- 963
- 964 Pomeroy, J.W., Gray, D.M. and Landine, P.G. The prairie blowing snow model: characteristics, validation, operation. *Journal of
965 Hydrology*, 144(1-4), pp.165-192, [https://doi.org/10.1016/0022-1694\(93\)90171-5](https://doi.org/10.1016/0022-1694(93)90171-5), 1993.
- 966
- 967 Rabier, F.: Overview of global data assimilation developments in numerical weather-prediction centres. *Quarterly Journal of the
968 Royal Meteorological Society: A journal of the atmospheric sciences, applied meteorology and physical oceanography*, 131(613),
969 pp.3215-3233, <https://doi.org/10.1256/qj.05.129>, 2005.
- 970
- 971 Rice, R. and Bales, R.C.: Embedded-sensor network design for snow cover measurements around snow pillow and snow course
972 sites in the Sierra Nevada of California. *Water Resources Research*, 46(3), <https://doi.org/10.1029/2008WR007318>, 2010.
- 973
- 974 Riemann, R., Wilson, B.T., Lister, A. and Parks, S.: An effective assessment protocol for continuous geospatial datasets of forest
975 characteristics using USFS Forest Inventory and Analysis (FIA) data. *Remote Sensing of Environment*, 114(10), pp.2337-2352,
976 <https://doi.org/10.1016/j.rse.2010.05.010>, 2010.
- 977



- 978 Rienecker, M.M., Suarez, M.J., Gelaro, R., Todling, R., Bacmeister, J., Liu, E., Bosilovich, M.G., Schubert, S.D., Takacs, L., Kim,
979 G.K. and Bloom, S.: MERRA: NASA's modern-era retrospective analysis for research and applications, *Journal of Climate*, 24(14),
980 pp.3624-3648, <https://doi.org/10.1175/JCLI-D-11-00015.1>, 2011.
- 981
- 982 Reges, H.W., Doesken, N., Turner, J., Newman, N., Bergantino, A. and Schwalbe, Z.: COCORAHs: The evolution and
983 accomplishments of a volunteer rain gauge network. *Bulletin of the American Meteorological Society*, 97(10), pp.1831-1846,
984 <https://doi.org/10.1175/BAMS-D-14-00213.1>, 2016.
- 985
- 986 Reichle, R.H., McLaughlin, D.B. and Entekhabi, D.: Hydrologic data assimilation with the ensemble Kalman filter. *Monthly*
987 *Weather Review*, 130(1), pp.103-114, [https://doi.org/10.1175/1520-0493\(2002\)130<0103:HDAWTE>2.0.CO;2](https://doi.org/10.1175/1520-0493(2002)130<0103:HDAWTE>2.0.CO;2), 2002.
- 988
- 989 Reichle, R.H.: Data assimilation methods in the Earth sciences. *Advances in water resources*, 31(11), pp.1411-1418,
990 <https://doi.org/10.1016/j.advwatres.2008.01.001/>, 2008.
- 991
- 992 Rivington, M., Matthews, K.B., Bellocchi, G. and Buchan, K.: Evaluating uncertainty introduced to process-based simulation
993 model estimates by alternative sources of meteorological data. *Agricultural Systems*, 88(2-3), pp.451-471,
994 <https://doi.org/10.1016/j.agsy.2005.07.004>, 2006.
- 995
- 996 Saha, S., Moorthi, S., Pan, H.L., Wu, X., Wang, J., Nadiga, S., Tripp, P., Kistler, R., Woollen, J., Behringer, D. and Liu, H.: The
997 NCEP climate forecast system reanalysis. *Bulletin of the American Meteorological Society*, 91(8), pp.1015-1058,
998 <https://doi.org/10.1175/2010BAMS3001.1>, 2010.
- 999
- 1000 Saha, S., Moorthi, S., Wu, X., Wang, J., Nadiga, S., Tripp, P., Behringer, D., Hou, Y.T., Chuang, H.Y., Iredell, M. and Ek, M.:
1001 The NCEP climate forecast system version 2. *Journal of Climate*, 27(6), pp.2185-2208, [https://doi.org/10.1175/JCLI-D-12-](https://doi.org/10.1175/JCLI-D-12-00823.1)
1002 [00823.1](https://doi.org/10.1175/JCLI-D-12-00823.1), 2014.
- 1003
- 1004 Schmucki, E., Marty, C., Fierz, C. and Lehning, M.: Evaluation of modelled snow depth and snow water equivalent at three
1005 contrasting sites in Switzerland using SNOWPACK simulations driven by different meteorological data input. *Cold Regions*
1006 *Science and Technology*, 99, pp.27-37, <https://doi.org/10.1016/j.coldregions.2013.12.004>, 2014.
- 1007
- 1008 Schaefer, M. and Woodyer, T.: Assessing absolute and relative accuracy of recreation-grade and mobile phone GNSS devices: a
1009 method for informing device choice. *Area*, 47(2), pp.185-196, <https://doi.org/10.1111/area.12172>, 2015.
- 1010
- 1011 Schneider, C., Laizé, C.L.R., Acreman, M.C. and Flörke, M.: How will climate change modify river flow regimes in Europe?.
1012 *Hydrology and Earth System Sciences*, 17(1), pp.325-339, <https://doi.org/10.5194/hess-17-325-2013>, 2013.
- 1013
- 1014 Schlögl, S., Marty, C., Bavay, M. and Lehning, M.: Sensitivity of Alpine3D modeled snow cover to modifications in DEM
1015 resolution, station coverage and meteorological input quantities. *Environmental modelling & software*, 83, pp.387-396,
1016 <https://doi.org/10.1016/j.envsoft.2016.02.017>, 2016.
- 1017
- 1018 Seibert, J., Strobl, B., Etter, S., Hummer, P. and van Meerveld, H.J.: Virtual staff gauges for crowd-based stream level observations.
1019 *Frontiers in Earth Science - Hydrosphere*, 7, p.70, <https://doi.org/10.3389/feart.2019.00070>, 2019.



- 1020
- 1021 Serreze, M.C., Clark, M.P., Armstrong, R.L., McGinnis, D.A. and Pulwarty, R.S.: Characteristics of the western United States
1022 snowpack from snowpack telemetry (SNOTEL) data. *Water Resources Research*, 35(7), pp.2145-2160,
1023 <https://doi.org/10.1029/1999WR900090>, 1999.
- 1024
- 1025 Shulski, M. and Wendler, G.: *The climate of Alaska*. University of Alaska Press, 2007.
- 1026
- 1027 Silvertown, J.: A new dawn for citizen science. *Trends in ecology & evolution*, 24(9), pp.467-471,
1028 <https://doi.org/10.1016/j.tree.2009.03.017>, 2009.
- 1029
- 1030 Sturm, M., Holmgren, J. and Liston, G.E.: A seasonal snow cover classification system for local to global applications. *Journal of*
1031 *Climate*, 8(5), pp.1261-1283, [https://doi.org/10.1175/1520-0442\(1995\)008<1261:ASSCCS>2.0.CO;2](https://doi.org/10.1175/1520-0442(1995)008<1261:ASSCCS>2.0.CO;2), 1995.
- 1032
- 1033 Sturm, M., Taras B., Liston G., Derksen, C., Jonas T., and Lea, J.: Estimating Snow Water Equivalent Using Snow Depth Data
1034 and Climate Classes. *Journal of Hydrometeorology* 11 (6): 1380–94. <https://doi.org/10.1175/2010JHM1202.1>, 2010a.
- 1035
- 1036 Sturm, M. and Wagner, A.M.: Using repeated patterns in snow distribution modeling: An Arctic example. *Water Resources*
1037 *Research*, 46(12), <https://doi.org/10.1029/2010WR009434>, 2010b.
- 1038
- 1039 Sturm, M.: White water: Fifty years of snow research in WRR and the outlook for the future. *Water Resources Research*, 51(7),
1040 pp.4948-4965, <https://doi.org/10.1002/2015WR017242>, 2015.
- 1041
- 1042 Trujillo, E., Molotch, N.P., Goulden, M.L., Kelly, A.E. and Bales, R.C.: Elevation-dependent influence of snow accumulation on
1043 forest greening. *Nature Geoscience*, 5(10), pp.705-709, <https://doi.org/10.1038/ngeo1571>, 2012.
- 1044
- 1045 van Meerveld, H. J. I., Vis, M. J. P., and Seibert, J.: Information content of stream level class data for hydrological model
1046 calibration, *Hydrol. Earth Syst. Sci.*, 21, 4895-4905, <https://doi.org/10.5194/hess-21-4895-2017>, 2017.
- 1047
- 1048 Viviroli, D., Dürr, H.H., Messerli, B., Meybeck, M. and Weingartner, R.: Mountains of the world, water towers for humanity:
1049 Typology, mapping, and global significance. *Water resources research*, 43(7), <https://doi.org/10.1029/2006WR005653>, 2007.
- 1050
- 1051 Wagner, W.: Investigating the snow climate of Turnagain Pass, Alaska. In *Proceedings of the International Snow Science*
1052 *Workshop*, Anchorage, AK (pp. 913-917), 2012.
- 1053
- 1054 Wiggins, A. and Crowston, K.: From conservation to crowdsourcing: A typology of citizen science. In 2011 44th Hawaii
1055 international conference on system sciences (pp. 1-10). IEEE, <https://doi.org/10.1109/HICSS.2011.207>, 2011.
- 1056
- 1057 Wilson, A.B., Bromwich, D.H. and Hines, K.M.: Evaluation of Polar WRF forecasts on the Arctic System Reanalysis domain: 2.
1058 Atmospheric hydrologic cycle. *Journal of Geophysical Research: Atmospheres*, 117(D4), <https://doi.org/10.1029/2010JD015013>,
1059 2012.
- 1060



1061 Wrzesien, M.L., Durand, M.T., Pavelsky, T.M., Howat, I.M., Margulis, S.A. and Huning, L.S.: Comparison of methods to estimate
1062 snow water equivalent at the mountain range scale: a case study of the California Sierra Nevada. *Journal of Hydrometeorology*,
1063 18(4), pp.1101-1119, <https://doi.org/10.1175/JHM-D-16-0246.1>, 2017.
1064
1065 Yeeles, A.: Citizen snow-scientists trek into the back country. *Nature Climate Change*, 8(11), p.944,
1066 <https://doi.org/10.1038/s41558-018-0329-0>, 2018.
1067
1068
1069